

Measurement and analysis of the ^{243}Am neutron capture cross section at the n_TOF facility at CERN

E. Mendoza,¹ D. Cano-Ott,¹ C. Guerrero,^{1,2} E. Berthoumieux,³ U. Abbondanno,⁴ G. Aerts,³ F. Álvarez-Velarde,¹ S. Andriamonje,³ J. Andrzejewski,⁵ P. Assimakopoulos,⁶ L. Audouin,⁷ G. Badurek,⁸ J. Balibrea,¹ P. Baumann,⁹ F. Bečvář,¹⁰ F. Belloni,⁴ F. Calviño,¹¹ M. Calviani,^{12,13} R. Capote,^{14,15} C. Carrapiço,^{16,3} A. Carrillo de Albornoz,¹⁶ P. Cennini,² V. Chepel,¹⁷ E. Chiaveri,² N. Colonna,¹⁸ G. Cortes,¹⁹ A. Couture,²⁰ J. Cox,²⁰ M. Dahlfors,² S. David,⁷ I. Dillmann,²¹ R. Dolfini,²² C. Domingo-Pardo,²³ W. Dridi,³ I. Duran,²⁴ C. Eleftheriadis,²⁵ L. Ferrant,⁷ A. Ferrari,² R. Ferreira-Marques,¹⁷ L. Fitzpatrick,² H. Fraiss-Koelbl,²⁶ K. Fujii,⁴ W. Furman,²⁷ I. Gonçalves,¹⁶ E. González-Romero,¹ A. Goverdovski,²⁸ F. Gramegna,¹² E. Griesmayer,²⁶ F. Gunsing,³ B. Haas,²⁹ R. Haight,³⁰ M. Heil,²¹ A. Herrera-Martinez,² M. Igashira,³¹ S. Isaev,³ E. Jericha,⁸ F. Käppeler,²¹ Y. Kadi,² D. Karadimos,⁶ D. Karamanis,⁶ V. Ketlerov,^{28,2} M. Kerveno,⁹ P. Koehler,³² V. Kononov,^{27,2} E. Kossionides,³³ M. Krtička,¹⁰ C. Lampoudis,^{25,3} H. Leeb,⁸ A. Lindote,¹⁷ S. Lo Meo,³⁴ I. Lopes,¹⁷ R. Lossito,² M. Lozano,¹⁵ S. Lukic,⁹ J. Marganec,⁵ L. Marques,¹⁶ S. Marrone,¹⁸ T. Martínez,¹ C. Massimi,³⁵ P. Mastinu,¹² A. Mengoni,^{14,2} P. M. Milazzo,⁴ C. Moreau,⁴ M. Mosconi,²¹ F. Neves,¹⁷ H. Oberhummer,⁸ S. O'Brien,²⁰ M. Oshima,³⁶ J. Pancin,³ C. Papachristodoulou,⁶ C. Papadopoulos,³⁷ C. Paradela,²⁴ N. Patronis,⁶ A. Pavlik,³⁸ P. Pavlopoulos,³⁹ L. Perrot,³ M. T. Pigni,⁸ R. Plag,²¹ A. Plompen,⁴⁰ A. Plukis,³ A. Poch,¹⁹ J. Praena,¹² C. Pretel,¹⁹ J. Quesada,¹⁵ T. Rauscher,^{41,42} R. Reifarth,³⁰ C. Rubbia,²² G. Rudolf,⁹ P. Rullhusen,⁴⁰ J. Salgado,¹⁶ C. Santos,¹⁶ L. Sarchiapone,² I. Savvidis,²⁵ C. Stephan,⁷ G. Tagliente,¹⁸ J. L. Tain,²³ L. Tassan-Got,⁷ L. Tavora,¹⁶ R. Terlizzi,¹⁸ G. Vannini,³⁵ P. Vaz,¹⁶ A. Ventura,⁴³ D. Villamarin,¹ M. C. Vicente,¹ V. Vlachoudis,² R. Vlastou,³⁷ F. Voss,²¹ S. Walter,²¹ H. Wendler,² M. Wiescher,²⁰ and K. Wisshak²¹

(n_TOF Collaboration)

¹CIEMAT, Centro de Investigaciones Energéticas Medioambientales y Tecnológicas, Madrid, Spain²CERN, Geneva, Switzerland³CEA/Saclay - IRFU, Gif-sur-Yvette, France⁴Istituto Nazionale di Fisica Nucleare, Trieste, Italy⁵University of Lodz, Lodz, Poland⁶University of Ioannina, Greece⁷Centre National de la Recherche Scientifique/IN2P3 - IPN, Orsay, France⁸Atominstytut der Österreichischen Universitäten, Technische Universität Wien, Austria⁹Centre National de la Recherche Scientifique/IN2P3 - IReS, Strasbourg, France¹⁰Charles University, Prague, Czech Republic¹¹Universidad Politécnica de Madrid, Spain¹²Istituto Nazionale di Fisica Nucleare, Laboratori Nazionali di Legnaro, Italy¹³Dipartimento di Fisica, Università di Padova, Italy¹⁴International Atomic Energy Agency (IAEA), Nuclear Data Section, Vienna, Austria¹⁵Universidad de Sevilla, Sevilla, Spain¹⁶Instituto Tecnológico e Nuclear (ITN), Lisbon, Portugal¹⁷LIP - Coimbra and Departamento de Física da Universidade de Coimbra, Coimbra, Portugal¹⁸Istituto Nazionale di Fisica Nucleare, Bari, Italy¹⁹Universitat Politècnica de Catalunya, Barcelona, Spain²⁰University of Notre Dame, Notre Dame, Indiana, USA²¹Karlsruhe Institute of Technology (KIT), Institut für Kernphysik, Karlsruhe, Germany²²Università degli Studi Pavia, Pavia, Italy²³Instituto de Física Corpuscular, CSIC-Universidad de Valencia, Spain²⁴Universidade de Santiago de Compostela, Spain²⁵Aristotle University of Thessaloniki, Greece²⁶Fachhochschule Wiener Neustadt, Wiener Neustadt, Austria²⁷Joint Institute for Nuclear Research, Frank Laboratory of Neutron Physics, Dubna, Russia²⁸Institute of Physics and Power Engineering, Kaluga region, Obninsk, Russia²⁹Centre National de la Recherche Scientifique/IN2P3 - CENBG, Bordeaux, France³⁰Los Alamos National Laboratory, Los Alamos, New Mexico, USA³¹Tokyo Institute of Technology, Tokyo, Japan³²Oak Ridge National Laboratory, Physics Division, Oak Ridge, Tennessee, USA³³NCSR, Athens, Greece³⁴ENEA, Bologna, Italy³⁵Dipartimento di Fisica, Università di Bologna, and Sezione INFN di Bologna, Italy³⁶Japan Atomic Energy Research Institute, Tokai-mura, Japan³⁷National Technical University of Athens, Greece³⁸Institut für Isotopenforschung und Kernphysik, Universität Wien, Austria³⁹Pôle Universitaire Léonard de Vinci, Paris La Défense, France

⁴⁰*CEC-JRC-IRMM, Geel, Belgium*⁴¹*Centre for Astrophysics Research, School of Physics, Astronomy and Mathematics, University of Hertfordshire, Hatfield, United Kingdom*⁴²*Department of Physics - University of Basel, Switzerland*⁴³*Istituto Nazionale di Fisica Nucleare, Bologna, Italy*

(Received 23 May 2014; revised manuscript received 1 July 2014; published 11 September 2014)

Background: The design of new nuclear reactors and transmutation devices requires to reduce the present neutron cross section uncertainties of minor actinides.

Purpose: Improvement of the $^{243}\text{Am}(n,\gamma)$ cross section uncertainty.

Method: The $^{243}\text{Am}(n,\gamma)$ cross section has been measured at the n_TOF facility at CERN with a BaF₂ total absorption calorimeter, in the energy range between 0.7 eV and 2.5 keV.

Results: The $^{243}\text{Am}(n,\gamma)$ cross section has been successfully measured in the mentioned energy range. The resolved resonance region has been extended from 250 eV up to 400 eV. In the unresolved resonance region our results are compatible with one of the two incompatible capture data sets available below 2.5 keV. The data available in EXFOR and in the literature have been used to perform a simple analysis above 2.5 keV.

Conclusions: The results of this measurement contribute to reduce the $^{243}\text{Am}(n,\gamma)$ cross section uncertainty and suggest that this cross section is underestimated up to 25% in the neutron energy range between 50 eV and a few keV in the present evaluated data libraries.

DOI: [10.1103/PhysRevC.90.034608](https://doi.org/10.1103/PhysRevC.90.034608)

PACS number(s): 25.40.Lw, 28.41.-i, 28.20.Np, 27.90.+b

I. INTRODUCTION

Nuclear data for minor actinides have gained importance in the last years because they are necessary for improving the design and performance of advanced nuclear reactors and transmutation devices for the incineration of radioactive nuclear waste [1–3]. In particular, ^{243}Am is the minor actinide which contributes most to the total radiotoxicity of the spent fuel at times after disposal close to its half-life (7370 yr). In addition, the $^{243}\text{Am}(n,\gamma)$ reaction produces ^{244}Cm , which is a strong neutron emitter and which is in the path of the creation of any heavier isotope by further neutron captures.

The differential data available for the evaluation of the ^{243}Am capture cross section are presented in Table I. There are only two differential capture measurements covering the energy region below 250 eV, apart from the one presented here. Both are recent and their final results have not been published

TABLE I. Differential measurements performed up to now relevant for the evaluation of the ^{243}Am capture cross section.

Reference	Type	Range (eV)
Belanova <i>et al.</i> (1976) [4]	Transmission	0.35–35
Simpson <i>et al.</i> (1974) [5]	Transmission	$0.5\text{--}1 \times 10^3$
Berreth <i>et al.</i> (1970) [6]	Transmission	0.008–25.6
Cote <i>et al.</i> (1959) [7]	Transmission	0.0014–15.44
Weston <i>et al.</i> (1985) [8]	Capture	$258\text{--}9.2 \times 10^4$
Wisshak <i>et al.</i> (1983) [9]	Capture	$5 \times 10^3\text{--}2.5 \times 10^5$
Jandel <i>et al.</i> (2009) [10] ^a	Capture	$8\text{--}2.5 \times 10^5$
Hori <i>et al.</i> (2009) [11] ^a	Capture	0.01–400
This work	Capture	$0.7\text{--}2.5 \times 10^3$
Kimura <i>et al.</i> (2012) [12] ^b	Capture	–
Alekseev <i>et al.</i> (2011) [13] ^b	Fission	–

^aNeither the yield nor the resulting cross sections have been published yet.

^bOnly the resonance parameters of the resonance at 1.35 eV (Kimura *et al.*) or below 17 eV (Alekseev *et al.*) are provided.

yet. In this energy range, only the information provided by the transmission measurements have been used to determine the ^{243}Am capture cross section in the current evaluated data libraries (the last releases at this moment are ENDF/B-VII.1 [14], JENDL-4.0 [15], JEFF-3.2 [16], ROSFOND-2010 [17], and CENDL-3.1 [18]). In particular, the present evaluations are based essentially on the results of Simpson *et al.* [5], which are the only data set extending above 35 eV. This information has been completed with the integral measurements presented in Table II, which provide the thermal capture cross section and resonance integral measurements performed up to now, all showing sizable discrepancies.

At higher neutron energies there are only two data sets between 250 eV and 5 keV, both of them carried out by Weston *et al.*, which differ significantly below 2 keV. In addition, the results of Wisshak *et al.* [9] are 10–15% lower than the data of Weston *et al.* [8] in the energy range of overlap. Together with these differential measurements, there are also integral measurements carried out in fast nuclear reactors, which provide information on the ^{243}Am capture cross section in the fast energy range. The results of the calculations performed with the evaluated libraries do not reproduce necessarily these experimental results [19,20]. These inconsistencies have motivated, for example, changes in the evaluated ^{243}Am capture cross section in the ENDF/B-VII.1 release with respect to ENDF/B-VII.0 [21].

The lack of data, the inconsistencies presented above, and the recent interest in the design of new nuclear devices, specially those related with the transmutation of the spent fuel, have motivated new ^{243}Am capture cross section measurements, such as the one presented in this work or by Jandel *et al.* [10] and Hori *et al.* [11].

The experimental setup of the $^{243}\text{Am}(n,\gamma)$ measurement carried out at the n_TOF facility at CERN is described in Sec. II. The procurement of the capture yield, which will be available in the EXFOR data base [34], is presented in Sec. III, followed by the cross section analysis in Sec. IV. At the end

TABLE II. Thermal capture cross sections (σ_0), resonance integrals [$I_0 = \int_{0.5\text{eV}}^{\infty} \sigma_\gamma(E)/E dE$] and ratios between them provided by different experiments and evaluations.

Reference	σ_0 (barn)	I_0 (barn)	I_0/σ_0
Hori <i>et al.</i> (2009) [11]	76.6 ^a	1970(110)	25.7(15)
Marie <i>et al.</i> (2006) [22]	81.8(36)		
Ohta <i>et al.</i> (2006) [23]		2250(300) ^b	
Hatsukawa <i>et al.</i> (1997) [24]	84.4		
Gavrilov <i>et al.</i> (1977) [25]	83(6)	2200(150)	26.5(26)
Simpson <i>et al.</i> (1974) [5]		1819(80) ^c	
Eberle <i>et al.</i> (1971) [26]	77(2)	1930(50) ^c	25.1(9)
Berreth <i>et al.</i> (1970) [6]	85(4)	1824(80) ^c	21.5(14)
Folger <i>et al.</i> (1968) [27]	78	2250 ^d	29
Bak <i>et al.</i> (1967) [28]	73(6)	2300(200)	32(4)
Ice (1966) [29]	66-84		
Butler <i>et al.</i> (1957) [30]	73.6(1.8)	2290(50)	31(1)
Harvey <i>et al.</i> (1954) [31]	140(50)		
Stevens <i>et al.</i> (1954) [32]	115		
Mughabghab (2006) [33]	75.1(18)	1820(70)	24.2(11)
ENDF/B-VII.1 [14]	80.4	2051	25.5
ENDF/B-VII.0 [21]	75.1	1820	24.2
JENDL-4.0 [15]	79.3	2040	25.7
JEFF-3.2 [16]	76.7	1788	23.3

^aValue assumed for normalization. I_0 is proportional to it.

^bThe thermal value of Marie *et al.* was assumed. The Ohta *et al.* measured value was $\hat{\sigma} = 174.5(5.3)$ barn and $\alpha = 0.0418(45)$, where $I_0 = \hat{\sigma}/\alpha + (0.45 - 1/\alpha)\sigma_0$.

^cCut-off energy was taken as 0.625 instead of 0.5 eV.

^dCut-off energy was taken as 0.83 instead of 0.5 eV.

of Sec. IV we extend the analysis of the $^{243}\text{Am}(n,\gamma)$ cross section up to higher energies with the data available in EXFOR and in the literature. Finally, the conclusions of this work are presented in Sec. V.

II. THE EXPERIMENTAL SETUP

A. The n_TOF facility at CERN

The n_TOF facility at CERN [35,36] is a pulsed neutron source coupled to a 200 m flight path designed to study neutron-nucleus interactions for neutron kinetic energies ranging from a few meV to several GeV. The neutrons are produced in spallation reactions by a 20 GeV/c proton beam with 16 ns FWHM time resolution and a repetition rate of ~ 0.4 Hz. During the experimental campaign of Phase-1 [37], the spallation source was a $80 \times 80 \times 60$ cm³ lead block surrounded by 5.8 cm of water, serving as a coolant and as a moderator for the initially fast neutron spectrum. The neutrons travel through an evacuated beam line with an angle of 10° with respect to the proton beam to the measuring station. Along the beam line a magnet avoids the charged particles reaching the measuring station and two collimators give the appropriate shape to the neutron beam. This facility is used mainly to measure fission and capture cross sections relevant for nuclear astrophysics and nuclear technologies.

Per nominal pulse of 7×10^7 protons there are about 1.5×10^5 neutrons between 1 eV and 10 keV reaching the

irradiation position, at 185 m from the spallation source, with a nearly isoenergetic energy distribution. Only proton pulses with intensities close to the mentioned nominal intensity have been considered in this analysis. At the irradiation position the neutron beam has a spatial distribution which does not vary significantly in the energy range of this measurement and that resembles a 2D-Gaussian with $\sigma_x = \sigma_y = 0.54$ cm [38]. The description of the resolution function can be found in Ref. [39].

B. The detection system

Three different detectors were used to determine the beam during the $^{243}\text{Am}(n,\gamma)$ measurement. The proton beam was characterized by a wall current monitor and wall current transformers [35], and the intensity of the neutron beam was measured with a silicon flux monitor [40]. The latter is a ^6Li -based Si detector system mounted about 2 m upstream of the sample.

The $^{243}\text{Am}(n,\gamma)$ reactions were recorded with the n_TOF total absorption calorimeter (TAC) [41] via the coincident detection of the prompt capture γ rays. The TAC, shown in Fig. 1, is a 4π segmented array made of 40 BaF₂ crystals with pentagonal and hexagonal shapes. Each crystal has been constructed by cutting a BaF₂ cylinder of 14 cm diameter and 15 cm length. For optimal light collection the crystals are covered with two layers of 0.1 mm thick teflon foil and an 0.1 mm thick polished aluminum sheet on the outside. In order to minimize the detection of scattered neutrons, the crystals are enclosed in 1 mm thick ^{10}B loaded carbon fiber capsules. Each capsule is coupled to an aluminum cylinder that houses a 12.7 cm Photonis XP4508B photomultiplier and a special voltage divider made at the Instituto Tecnológico e Nuclear in Lisbon that favors its fast recovery. The complete modules are attached to an aluminum honey comb structure that holds the complete assembly. The TAC is divided in two hemispheres

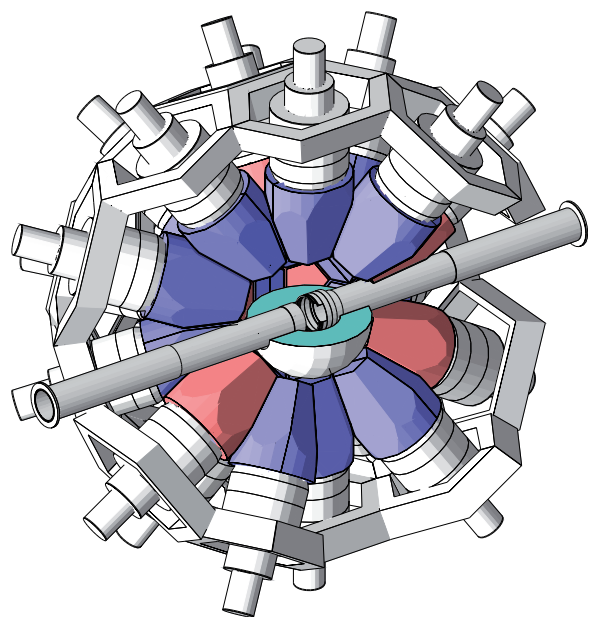


FIG. 1. (Color online) Schematic view of the n_TOF total absorption calorimeter.

that can be opened and closed, and form a spherical shell of 10 cm inner radius and 25 cm outer radius, approximately, covering around 95% of the entire solid angle. A neutron absorber consisting of a 5 cm thick spherical shell made of $\text{Li}_2\text{C}_{12}\text{H}_{20}\text{O}_4$ was covering the inner surface of the TAC to enforce the effect of the ^{10}B loaded carbon fiber capsules.

The detector signals were recorded with a multichannel data acquisition system [42] based on Acqiris-DC270 digitizers with 8 bits resolution operating at 250 MHz. With that system each pulse could be followed for a time interval of 16 ms, storing the digitized electronic response of each detector module for all neutron energies above 0.7 eV. The data buffers were analyzed offline with dedicated pulse shape reconstruction algorithms. The algorithm used to analyze the BaF_2 signals is described in Ref. [43], and a more accessible reference of a similar routine is [44]. It returns for each signal the time of flight, the area, and other parameters used to distinguish the detected particle type: γ or α (the latter is produced by the decay of Ra impurities in the crystals). Each detector was calibrated in energy from measurements performed with standard γ -ray sources (^{137}Cs , ^{60}Co , ^{88}Y , ^{24}Na , and Pu/C). Throughout the entire measurement, gain drifts were monitored via the line peaks in the α spectra of each BaF_2 module. The individual detector signals are grouped into TAC events using a coincidence window of 20 ns. Each TAC event is characterized by its time of flight, total deposited energy (E_{sum}) and crystal multiplicity (m_{cr}), which is the number of detector modules contributing to an event. The E_{sum} and m_{cr} values are used to apply conditions to the detected events in order to improve the capture to background ratio. In this paper, the word *event* always refers to these TAC events.

C. The ^{243}Am and auxiliary samples and measurements

The ^{243}Am sample was manufactured at IPPE Obninsk (Russia) in February 2004. It was in form of oxide powder (AmO_2) deposited on an Al backing 10 mm in diameter and less than 70 mg in mass, according to the specifications provided by the manufacturers. The sample was encapsulated in a Ti canning 15 mm in diameter and 0.17 and 0.18 mm thickness above and below the sample. The total weight of the sample (AmO_2 , Al backing, and Ti canning) was 420.9(1) mg. According to the specifications provided by the manufacturers, the total mass of the AmO_2 deposit was 11.3 mg, and the isotopic mass of ^{243}Am , 10.0 mg. However, this value is at odds with a spectroscopic characterization of the sample performed at CERN, which resulted in an ^{243}Am mass of 7.34(1.10) mg, as well as with a separate measurement of the sample activity, which yielded a mass of 6.77(1.02) mg. In view of these differences, the data were finally normalized to the transmission measurements available in EXFOR (see Sec. III C), especially to the one performed by Simpson *et al.* [5], obtaining a normalization uncertainty of 3%, and an associated sample mass of 6.23 ($\pm 4\%$) mg, which is in agreement with the spectroscopic measurements. The impurities were determined during the resonance analysis process, resulting in 0.048 mg of ^{241}Am and 0.0025 mg of ^{240}Pu . The temperature of the sample was assumed to be

TABLE III. Number of pulses and protons dedicated to each measurement.

Measurement	no. of pulses	no. of protons
^{243}Am	1.86×10^5	1.27×10^{18}
Env. background	1.37×10^4	–
Activity	1.53×10^4	–
^{197}Au	2.19×10^4	1.53×10^{17}
Graphite	3.76×10^3	2.67×10^{16}
Ti canning	1.49×10^3	1.04×10^{16}
Empty frame	4.16×10^3	2.94×10^{16}

293 ± 4 K, which is the average temperature of the n_TOF experimental area.

The sample was placed in the center of the TAC, held by two kapton foils $25 \mu\text{m}$ in thickness and surrounded by the neutron absorber. Due to the high sample activity, an 11.5 cm long and 1 mm thick layer of Pb was placed around the evacuated neutron flight path at the position of the sample. In this way, the amount of γ rays originated in the sample decay and reaching the TAC was strongly reduced. However, even with this lead shielding, the counting rate was much higher than of other previous measurements performed with the TAC [45,46].

Three other samples were also measured for the determination of the $^{243}\text{Am}(n,\gamma)$ cross section. An empty Ti-Al canning with the same diameter but a slightly different mass of 455.4(1) mg was used to measure the background due to the sample canning, a graphite sample 10 mm in diameter and 70.0(1) mg in mass served to determine the TAC response to sample scattered neutrons, and a ^{197}Au sample 10 mm in diameter and 185.4(1) mg in mass was used to determine the fraction of the beam intercepted by the ^{243}Am sample, and also for validating the analysis procedure.

Additional measurements dedicated to the background problem were performed: (i) without beam and without sample (Env. Background), (ii) without beam but with the sample in place (Activity), and (iii) with neutron beam but without any sample (Empty frame). The time (pulses) and beam intensity (protons) allocated to each of these measurements is summarized in Table III.

III. DATA REDUCTION

The experimental capture yield can be calculated as

$$Y_{n,\gamma}(E_n) = \frac{C_{\text{tot}}(E_n) - C_{\text{bkg}}(E_n)}{\varepsilon \times F_{\text{BIF}} \times \phi(E_n)}, \quad (1)$$

where $C_{\text{tot}}(E_n)$ and $C_{\text{bkg}}(E_n)$ are the number of total and background counts registered by the TAC, respectively, under certain E_{sum} and m_{cr} conditions, ε is the corresponding detection efficiency, $\phi(E_n)$ the intensity of the neutron beam, and F_{BIF} the fraction of the neutron beam intercepted by the measured sample.

The data reduction process is quite similar to the one described in Ref. [46], with some additional features especially developed to deal with the much higher counting rates (5.4 events/ μs) of the $^{243}\text{Am}(n,\gamma)$ measurement due to the sample activity.

A. Background and selection of the analysis conditions

The background events in the $^{243}\text{Am}(n,\gamma)$ measurement can be divided into two contributions: (i) events coming from fission reactions and scattered neutrons in the ^{243}Am nuclei; and (ii) the rest of the background, which results from the environmental background, the activity of the BaF_2 crystals, the sample activity and the interaction of the neutron beam with all the materials except with the ^{243}Am nuclei.

In principle, the second contribution could be obtained directly from the different background measurements summarized in Table III. However, these background components were distorted in the ^{243}Am measurement by additional pile-up and dead time effects due to the high sample activity. Therefore, the background cannot be adopted from the dedicated measurements but requires some corrections. As described in detail in Ref. [47], the corresponding procedure is based on the offline manipulation of the digitized detector signals and the parametrization of the response of the pulse shape analysis routine.

The deposited energy spectrum obtained from the $^{243}\text{Am}(n,\gamma)$ measurement in the neutron energy range 1–10 eV is presented in Fig. 2, together with different background contributions: the total contribution (dummy sample), the total contribution except the one related with the interaction of the neutron beam with the Ti capsule (sample out), and the contribution not related with the neutron beam (No beam). The part of the spectra below ~ 2 MeV corresponds mostly to sample activity events, whereas above 6 MeV the events are due to background related to the neutron beam, because the total energy of the γ cascade after neutron capture in ^{243}Am cannot exceed the neutron separation energy of the compound nucleus, $S_n(^{244}\text{Am}) = 5.36$ MeV, and the no-beam background events have lower energies. For this reason, the dummy sample spectrum should match the ^{243}Am spectrum above $E_{\text{sum}} = 6$ MeV as is the case if the pile-up corrections are properly applied (bottom panel of Fig. 2).

The capture to background ratio is highly improved if the low ($E_{\text{sum}} < 2$ MeV) and high ($E_{\text{sum}} > 6$ MeV) energy events are excluded from further analysis. This holds also for restrictions on m_{cr} , because capture events have, in general, higher multiplicity than the background. On the other hand, the detection efficiency becomes lower as the conditions in E_{sum} and m_{cr} become more restrictive. A detailed analysis led to the optimum conditions of $m_{\text{cr}} > 2$ and $2.5 < E_{\text{sum}} < 6$ MeV, which were adopted in the present analysis. The number of events detected per proton pulse under these conditions is presented in Fig. 3 as a function of the neutron energy. The background is smooth until $E_n = 2$ –3 keV, where the resonances of the Ti capsule appear, which are limiting this measurement to the energy region below 2.5 keV. The low-energy limit of 0.7 eV is given by the 16 ms recording time.

Due to small differences in the energy calibration caused by the pile-up correction method [48], there was a background component constant in time that could not be determined from the measurements and had to be fitted. The uncertainty due to this fit can be expressed by considering the background $B(E_n)$ as $B(E_n) + a/\sqrt{E_n}$, where $a = 0 \pm 3 \times 10^{-5} \sqrt{\text{eV}}$. The relative uncertainty of the background due to this component

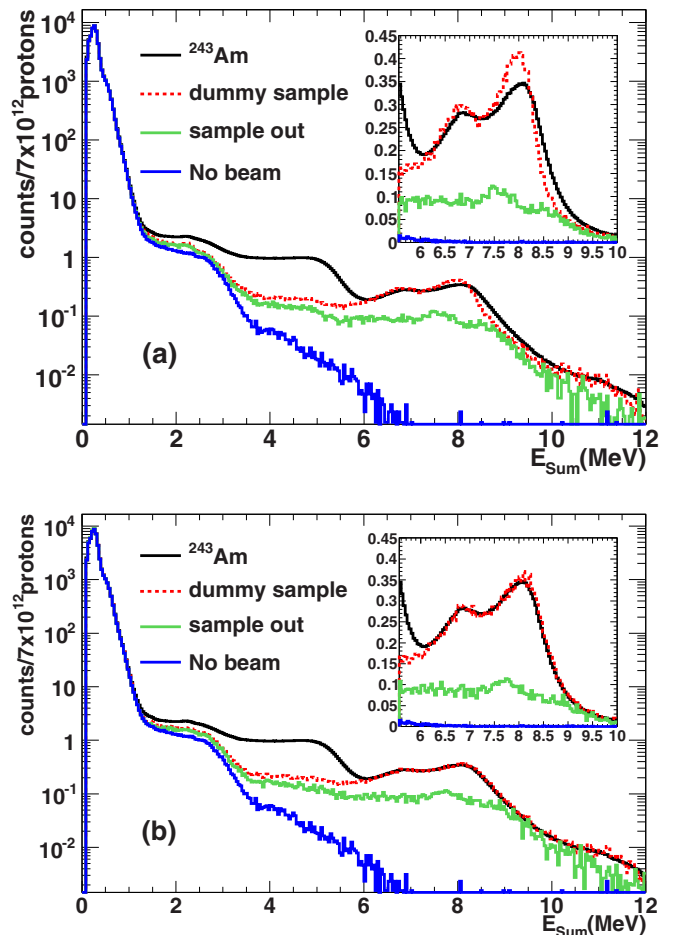


FIG. 2. (Color online) Deposited energy spectrum of the $^{243}\text{Am}(n,\gamma)$ measurement together with different background contributions, without any condition on m_{cr} . The top and bottom panels show the cases when pile-up corrections are neglected (a) and properly applied (b) in the calculation of the backgrounds, respectively. The effect is highlighted on a linear scale in the insets. The data correspond to neutron energies between 1 and 10 eV.

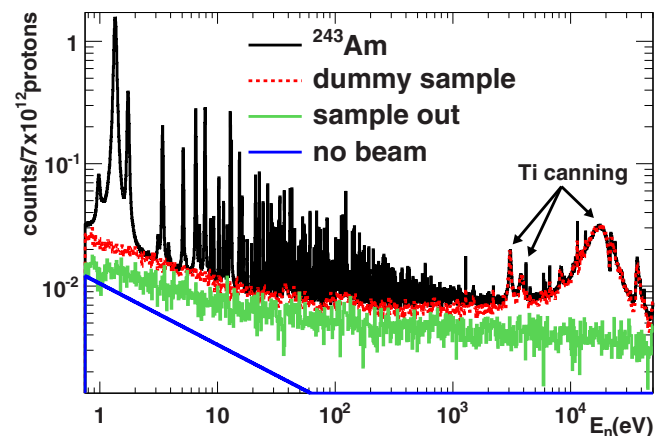


FIG. 3. (Color online) Number of events detected in the $^{243}\text{Am}(n,\gamma)$ measurement as a function of the neutron energy, together with different background contributions and under the conditions of $m_{\text{cr}} > 2$ and $2.5 < E_{\text{sum}} < 6$ MeV.

is 1%, 0.6%, 0.3%, and 0.13% at 1, 10, 100, and 1000 eV, respectively.

The background due to fission and neutron scattering in the ^{243}Am nuclei follows a similar resonant behavior as the $^{243}\text{Am}(n,\gamma)$ cross section. An estimation of this contribution can be performed with evaluated cross sections if the probability of detecting a scattered neutron (neutron sensitivity, in this paper) and a fission reaction are known. An estimation of the neutron sensitivity has been obtained from the measurement performed with the graphite sample (Table III), by assuming that the response of the TAC to neutrons scattered in carbon does not differ too much to the response to neutrons scattered in ^{243}Am . The neutron sensitivity depends on neutron energy and also on the E_{sum} and m_{cr} conditions. With the conditions used in this analysis, the 2.2 MeV γ rays from neutron capture in the H of the neutron absorber are mostly avoided, thus reducing the neutron sensitivity significantly. This obtained neutron sensitivity was used, together with the evaluated ^{243}Am cross section from the ENDF/B-VII.0 library, to estimate the background induced by neutron scattering in the AmO_2 sample. It was found that this component contributes less than 0.5% to the total background in the entire energy range of interest, even in the peak of the resonances. Assuming a conservatively high detection efficiency for fission events of 100%, this contribution would be higher than for scattering in the peak of certain ^{243}Am resonances, but would always be below 1% with respect to the capture yield. As a consequence, both contributions, elastic scattering and fission in the sample, have been neglected in the analysis.

B. Detection efficiency and determination of the sample activity

The detection efficiency has been calculated from Monte Carlo simulations. The process starts with the generation of the γ -ray cascades following neutron capture, which has been performed with the DECAYGEN code [49]. The resulting cascades are then transported into the TAC geometry with a code based on the GEANT4 package [50]. In the last step the Monte Carlo results are reconstructed in the same way as in a real experiment, including all the experimental effects such as the energy resolution of the crystals or the dead time and pile-up effects. The generation of the capture cascades is based on statistical models for the description of the level densities and photon strength functions. These models depend on parameters, which are adjusted until the experimental results are reproduced. A detailed description of the entire process is given in Ref. [51], and this method has been also used in Ref. [46]. The main difference with respect to [46] is that a new dead time and pile-up correction method was developed, especially to deal with the strong effect of the high sample activity [47].

The level density and photon strength function parameters have been adjusted to reproduce: (i) the deposited energy (E_{sum}) spectra for different detection multiplicities (m_{cr}); and (ii) the individual γ -ray energy spectra contributing to events with $4 < E_{\text{sum}} < 6$ MeV, where most of the capture cascade has been detected. The quality of the results is illustrated in Fig. 4 at the example of the spectra taken in the strongest ^{243}Am resonance at 1.35 eV, where the capture to background ratio is maximum.

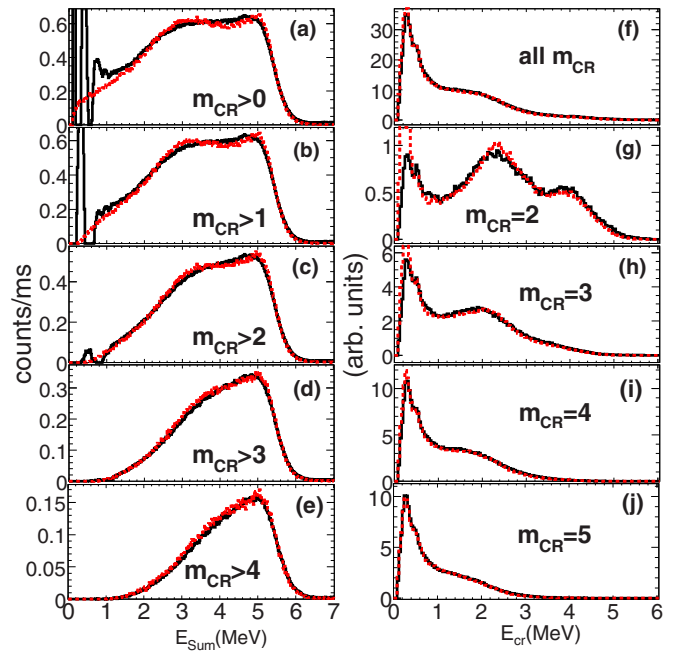


FIG. 4. (Color online) Experimental (solid lines) and simulated (dotted lines) deposited energy spectra from ^{243}Am capture cascades for different multiplicities. On the left (a)–(e), the total γ -ray energy spectra deposited in the TAC (E_{sum}). On the right (f)–(j), the individual crystal energy spectra obtained by gating on the total γ -ray energy in the $4 < E_{\text{sum}} < 6$ MeV region. The spectra have been obtained from the strongest ^{243}Am resonance at 1.35 eV. The oscillations present in some spectra at low energies are related with the background subtraction.

We have not found any significant difference in the shape of the deposited energy spectra between several resonances, and thus it was assumed that the detection efficiency depends only on the analysis conditions for E_{sum} and m_{cr} as well as on the counting rate CR via the pile-up and dead time corrections. This means that variations of the detection efficiency $\varepsilon = \varepsilon(E_{\text{sum}}, m_{\text{cr}}, CR)$ with neutron energy are only caused by the counting rate. The Monte Carlo simulations allowed us to determine the detection efficiency for any E_{sum} and m_{cr} conditions, and for any detected counting rate. For the conditions used in this analysis, $2.5 < E_{\text{sum}} < 6$ MeV and $m_{\text{cr}} > 2$, the detection efficiency for low counting rates is 56.3(12)% and varies by less than 1% in the entire neutron energy range of the analysis. The uncertainty of the efficiency was estimated from the uncertainties associated with the generation of capture cascades and of the simulated TAC geometry as described in Refs. [52,53].

The same tools used to calculate the detection efficiency were used to reproduce the energy response of the TAC to the sample activity. In this way, the ^{243}Am mass could be determined to 6.77 mg by comparison of the simulations and the data, consistent within the estimated 15% uncertainty with the 7.34 mg obtained by the spectroscopic characterization at CERN, but not with the value provided by the manufacturers (10 mg). An example of the comparison between the experimental and the simulated results is given in Fig. 5. The estimated uncertainty is much larger than the one of the

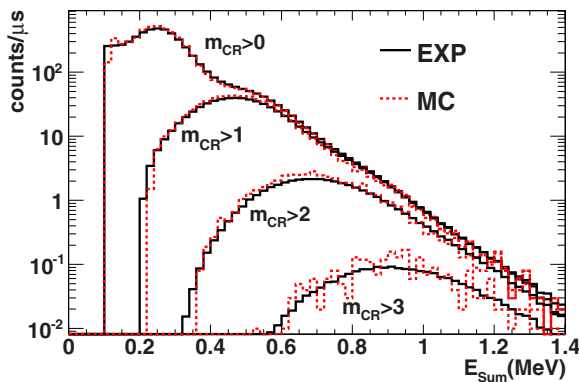


FIG. 5. (Color online) Experimental (solid lines) and simulated (dotted lines) deposited energy spectra due to the detection of the sample activity. A sample mass of 6.77 mg of ^{243}Am has been used.

detection efficiency due to the lower energies of the γ rays involved in the simulation, which in this case are close to the 100 keV threshold of the BaF_2 crystals.

C. Normalization

The fraction of the neutron beam intercepted by the sample, F_{BIF} , is the other quantity, together with the detection efficiency and the sample mass, which determines the normalization of the measurement. It has been obtained by replacing the ^{243}Am sample by a thick ^{197}Au sample of the same diameter (Sec. II C). The strongest ^{197}Au resonance at 4.9 eV has been used to measure the F_{BIF} by means of the saturated resonance method [54] obtaining a value of 0.196(3), which is consistent with other measured values [38,46] for the same sample diameter.

The uncertainty in the normalization of the experimental capture yield is dominated by the uncertainties in the detection efficiency (2.2%) and in the F_{BIF} (1.5%), which added linearly or quadratically give total uncertainties of 3.7% or 2.7%, respectively. Because the uncertainty of the sample mass is much larger (11%, if the average of the two obtained mass values is considered), the n_{TOF} measurement was finally normalized to the previous existing transmission measurements (Table I). The normalization procedure was performed with the SAMMY code [39], by fitting the obtained capture yield to the existing transmission data. Two different methods were used:

- (i) A simultaneous fit of the n_{TOF} capture yield and the transmission measurements, where the resonance parameters and the normalization of the n_{TOF} capture yield were varied. Only the data sets of Simpson *et al.* [5] were used for these analyses due to the lack of experimental information in the other transmission measurements.
- (ii) A normalization of the n_{TOF} data to the resonance parameters provided by the experimentalists of the transmission measurements [4–7] or the evaluators [33,55].

The transmission measurement of Simpson *et al.* was performed with two samples, one thicker [56] than the other [57].

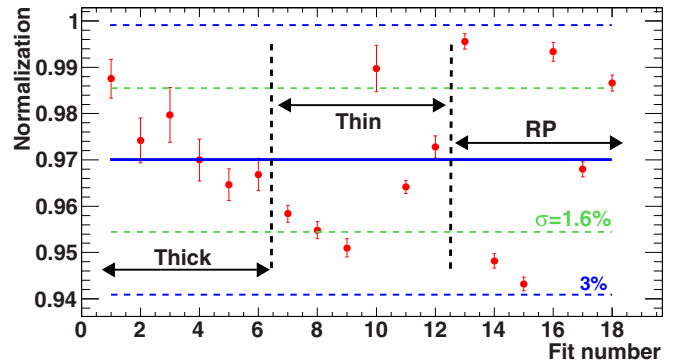


FIG. 6. (Color online) Normalization factors obtained in 18 different fits with SAMMY. In all cases, the initial thickness of the ^{243}Am sample considered was 2×10^5 atoms/barn, which corresponds to a mass of 6.34 mg.

The normalization of the n_{TOF} capture data was performed to both data sets in six different energy ranges [58]. For two reasons these transmission data were only used to normalize the capture data, and not to perform the resonance analysis. First, the uncertainties in the transmission data available in EXFOR are missing. Although it was estimated that reasonable assumptions could be made for the normalization, these were not sufficient to perform a resonance analysis. Second, the resolution function of the measurement was not given and had to be taken from a different reference. Therefore, the normalization was performed only at low neutron energies, below 50 eV, where the effect of the resolution function is very small.

In the second method we fitted the n_{TOF} capture yield to the theoretical capture yield obtained with resonance parameters provided by different experimentalists and evaluators. We found that our data are incompatible with the values provided by Cote *et al.* [7] and Belanova *et al.* [4] (see Table I), but are in a reasonable agreement with the resonance parameters provided by Simpson *et al.* [5], Berreth *et al.* [6], and some evaluations such as the ones performed by Mughabghab [33] or Maslov *et al.* [55].

The normalization values are presented in Fig. 6. The first and second set of six data points correspond to the fits based on the data of Simpson *et al.* taken with the thick and thin transmission samples, respectively, and the last six values were obtained with the other resonance parameters mentioned before. In all cases, the fits were performed above 3 eV, to avoid the strongest ^{243}Am resonance at 1.35 eV, where the self-shielding corrections are relevant (see Sec. IV A). The uncertainties in the normalization factors are due to the uncertainty in the background component constant in time presented in Sec. III A, which is the dominant contribution to the total uncertainty. More information concerning the normalization procedure can be found in Ref. [53].

The mean value of all normalization factors presented in Fig. 6 is 0.970, which corresponds to a sample thickness of 1.94×10^5 atoms/barn, or a mass of 6.23 mg of ^{243}Am . The standard deviation is 1.6%, but the different values are not independent and thus a 3% uncertainty was conservatively

adopted for the normalization of the capture cross section. In the calculation of the uncertainty of the sample mass, the 2.7% uncertainty due to the detection efficiency and the F_{BIF} has to be added. Thus, the fitted sample mass (or thickness) has an uncertainty of 4%, if both quantities are added quadratically.

IV. CROSS SECTION ANALYSIS

A. Analysis of the resolved resonance region

The resolved resonance region (RRR) has been analyzed with the SAMMY code (version 7.0.0) up to 400 eV (250 eV is the high energy limit of the RRR in the present evaluations). We have fitted the energy E_0 , the neutron width Γ_n , and the radiative capture width Γ_γ of each resonance in the measured energy range, using the Reich-Moore approximation. The resonance parameters of the negative and the first resonance at 0.415 eV, the scattering radius, and all fission widths were fixed to the values in the ENDF/B-VII.0 evaluation, after verifying that strong variations of these parameters do not affect the resulting capture yield significantly. It was confirmed by the techniques described in Ref. [59] that all the resonances observed in the investigated energy range were *s*-wave resonances. As it was not possible to distinguish the total spin values $J = 2, 3$, only the $g\Gamma_n$ values were determined. The time-energy relation was obtained by fitting the n_TOF time of flight distance to reproduce the energies of the resonances of ^{197}Au in the ENDF/B-VII.0 evaluation, obtaining 184.878 m. The n_TOF capture yield is presented together with the results of the SAMMY fit in Fig. 7, for several neutron energy ranges.

We have obtained the statistical uncertainties in the resonance parameters from SAMMY, together with their correlations. Concerning the systematic uncertainties, the following contributions were considered:

- (i) Uncertainties due to the normalization. These were estimated by performing 1000 fits with different normalization factors, which were randomly chosen according to a Gaussian distribution with standard deviation equal to the 3% uncertainty in the normalization. The systematic uncertainty of each fitted parameter was then estimated as the standard deviation of all the fitted values.
- (ii) Uncertainties due to the temperature of the sample. These were estimated in the same way as in the previous case, by performing 1000 fits with different temperatures, randomly varied according to a Gaussian distribution with mean and standard deviation equal to the sample temperature and its uncertainty, 293 ± 4 K, respectively.
- (iii) Uncertainties due to the background component constant in time (Sec. III A). They were estimated in the same way as in the two previous cases, by varying the parameter $a = 0 \pm 3 \times 10^{-5} \sqrt{eV}$ within its uncertainty.
- (iv) Uncertainty due to the shape of the background. Due to the low beam time dedicated to the background measurements (Table III), it was necessary to integrate the background in large neutron energy intervals to

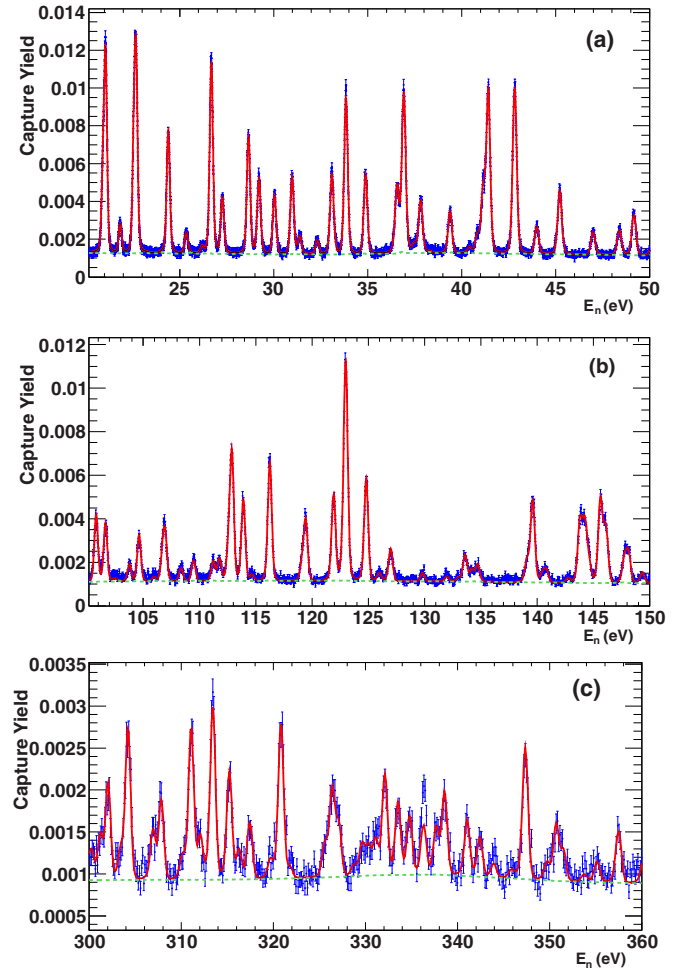


FIG. 7. (Color online) Examples of the fitted n_TOF capture yield, in different energy ranges. The dashed line corresponds to the overall background considered in SAMMY.

reduce the statistical fluctuations. Because the shape of the background was free of significant fluctuations we assumed a smoothed background for the resonance analysis. In order to estimate the uncertainties in the resonance parameters several analyses were performed using different smoothing techniques. The uncertainties in the fitted resonance parameters were then estimated as the standard deviation of the resulting values.

- (v) Uncertainty due to the Doppler broadening model. Following the same approach than in the previous cases, we estimated this contribution by comparing the results of a fit performed with the free gas model and a fit performed with the crystal-lattice model used in the SAMMY code [39]. In the latter case, we used the phonon spectrum of UO_2 , since it has not been measured for AmO_2 .
- (vi) Uncertainty due to sample inhomogeneities. The resonance integral $I_0 = \int_{0.5 \text{ eV}}^{\infty} \sigma_\gamma(E)/E dE$ obtained after performing the fit is $I_0 = 1681$ barn, which is significantly lower than any of the measured values presented in Table II. This discrepancy can be explained with

TABLE IV. Resonance parameters below 43 eV, together with their statistical uncertainties (σ_{stat}), their total systematic uncertainties (σ_{sys}) in the case of the Γ_γ parameters, and the sum of the systematic uncertainties with the exception of the one due to the normalization (σ_{sys^*}) in the case of the $g\Gamma_n$ parameters. All the $g\Gamma_n$ values have an additional 3% systematic uncertainty due to the normalization which has not been included in σ_{sys^*} .

E_0 (eV)	$g\Gamma_n$ (meV)	σ_{stat} (meV)	σ_{sys^*} (meV)	Γ_γ (meV)	σ_{stat} (meV)	σ_{sys} (meV)
-2	0.5735			39		
0.4151	0.00042			39		
0.9798	0.00643	0.00004	0.00008	34.4	0.4	1.1
1.3526	0.48579	0.00024	0.02447	48.57	0.04	2.50
1.7395	0.11465	0.00015	0.00111	40.11	0.12	0.39
3.1251	0.00486	0.00012	0.00015	34.0	2.4	1.8
3.4160	0.1389	0.0003	0.0007	39.93	0.24	0.47
3.8382	0.00608	0.00017	0.00022	45.2	2.9	2.4
5.1122	0.1512	0.0005	0.0007	40.2	0.4	0.6
6.5378	0.4824	0.0011	0.0031	41.0	0.3	0.7
7.0467	0.0359	0.0005	0.0004	47.8	2.1	1.3
7.8434	0.6813	0.0015	0.0048	42.9	0.3	0.8
8.3658	0.00788	0.00036	0.00016	42		
8.7480	0.0630	0.0008	0.0005	45.5	1.8	1.2
9.2931	0.0745	0.0008	0.0006	40.3	1.6	1.3
10.286	0.2384	0.0013	0.0009	53.5	0.9	1.0
10.870	0.00769	0.00046	0.00016	42		
11.249	0.1458	0.0013	0.0007	41.1	1.4	1.0
11.661	0.0518	0.0010	0.0004	40.8	2.8	0.8
12.098	0.0855	0.0012	0.0006	42.3	2.2	1.0
12.846	1.189	0.004	0.008	43.5	0.5	0.9
13.124	0.713	0.003	0.003	46.1	0.8	1.7
15.098	0.03001	0.00115	0.00019	42		
15.369	0.6881	0.0032	0.0021	44.0	0.9	1.3
16.178	0.2725	0.0024	0.0010	44.9	1.6	1.2
16.543	0.0978	0.0015	0.0004	42		
17.830	0.1115	0.0017	0.0005	42		
18.120	0.0200	0.0011	0.0003	42		
19.496	0.1089	0.0019	0.0006	42		
19.869	0.0425	0.0015	0.0005	42		
20.933	0.2356	0.0040	0.0006	42		
21.071	0.5822	0.0054	0.0018	42.8	1.7	1.3
21.840	0.0657	0.0028	0.0004	42		
21.851	0.02369	0.00224	0.00006	42		
22.580	0.3509	0.0064	0.0011	41.8	2.7	0.8
22.695	0.5875	0.0070	0.0014	42.5	2.0	1.5
24.404	0.4761	0.0045	0.0017	50.6	2.0	1.4
25.365	0.0797	0.0024	0.0006	42		
26.208	0.0257	0.0017	0.0003	42		
26.695	0.8469	0.0062	0.0020	44.6	1.6	1.4
27.284	0.2452	0.0041	0.0011	46.2	3.3	0.9
28.673	0.5589	0.0057	0.0015	45.3	2.3	1.3
29.230	0.3650	0.0051	0.0012	45.3	2.9	1.2
30.058	0.2916	0.0043	0.0009	42		
30.994	0.4023	0.0055	0.0014	42.6	2.9	1.4
31.406	0.0937	0.0033	0.0006	42		
32.339	0.0768	0.0031	0.0007	42		
33.115	0.4816	0.0064	0.0016	51.5	3.1	1.2
33.862	0.9399	0.0082	0.0020	40.6	2.0	1.8
34.908	0.4928	0.0064	0.0012	42		
36.583	0.4657	0.0086	0.0014	64	4	3

TABLE IV. (Continued.)

E_0 (eV)	$g\Gamma_n$ (meV)	σ_{stat} (meV)	σ_{sys^*} (meV)	Γ_γ (meV)	σ_{stat} (meV)	σ_{sys} (meV)
36.940	1.1680	0.0113	0.0020	57	3	3
37.498	0.0532	0.0035	0.0003	42		
37.837	0.3786	0.0071	0.0015	54.8	4.0	1.2
39.399	0.3007	0.0061	0.0011	42		
40.438	0.0456	0.0033	0.0005	42		
40.861	0.1369	0.0054	0.0007	42		
41.165	0.4730	0.0096	0.0007	42		
41.438	1.342	0.013	0.003	44.5	2.7	2.1
42.845	1.493	0.014	0.003	43.5	2.2	2.3

the existence of inhomogeneities in the sample, which would affect the self shielding and multiple scattering corrections. The strongest resonance at 1.35 eV is the only one where these corrections are important ($\sim 15\%$), and this resonance contributes around 70–80% to the resonance integral. In the rest of the resonances the self-shielding and multiple scattering corrections are much lower (eight resonances with corrections between 3% and 1%, the rest of the resonances below 1%). For this reason, we think that we can not trust the resonance parameters obtained for the strongest resonance at 1.35 eV. This is why the normalization to the transmission data was performed above 3 eV. In order to estimate the uncertainties due to the sample inhomogeneities, we compared the results of a fit performed with the nominal sample thickness with a fit in which the self-shielding and multiple scattering corrections were calculated for a sample with double thickness.

The rest of the contributions to the overall uncertainty, such as the ones corresponding to the dead time corrections or the resolution function, were considered to be negligible.

The values of the fitted resonance parameters are presented in Tables IV and V. The Γ_γ values with statistical uncertainties larger than 10% were fixed to the average radiative capture width, which was calculated from the rest of the values, all of them from resonances below 43 eV. Table IV provides the (quadratic) sum of the systematic uncertainties as well. In the case of the $g\Gamma_n$ parameters, the contributions to the systematic uncertainties associated with the temperature, the shape of the background and the Doppler broadening are negligible. In addition, since for nuclei with $\Gamma_\gamma \gg \Gamma_n$ the resonance area is nearly proportional to $g\Gamma_n$, the uncertainty in the $g\Gamma_n$ values due to the normalization is the same 3% as the normalization uncertainty and has not been included in the tables. Thus, only the uncertainties due to the background component constant in time and the sample inhomogeneities were taken into account in the tabulated values. Concerning the Γ_γ parameters, the normalization is the only negligible contribution to the total systematic uncertainty.

Above 43 eV, all Γ_γ values were fixed to $\langle \Gamma_\gamma \rangle = 42$ meV, and only the energies and $g\Gamma_n$ values are given in Table V. At these energies, the estimated uncertainties due to the

TABLE V. Resonance energies and $g\Gamma_n$ parameters between 43 and 400 eV together with the statistical uncertainties (σ_{stat}). All $g\Gamma_n$ values carry an additional systematic uncertainty of 3% due to the normalization.

E_0 (eV)	$g\Gamma_n \pm \sigma_{\text{stat}}$ (meV)	E_0 (eV)	$g\Gamma_n \pm \sigma_{\text{stat}}$ (meV)
44.016	0.2311 ± 0.0064	45.242	0.5887 ± 0.0092
47.018	0.2125 ± 0.0067	48.418	0.2416 ± 0.0073
49.189	0.4093 ± 0.0088	50.107	0.058 ± 0.006
51.144	0.507 ± 0.010	52.026	0.039 ± 0.006
52.916	1.043 ± 0.014	53.579	0.035 ± 0.007
53.868	0.325 ± 0.010	54.393	0.871 ± 0.015
54.617	0.153 ± 0.011	55.737	0.912 ± 0.014
57.194	0.051 ± 0.007	58.572	0.200 ± 0.010
58.953	0.447 ± 0.012	59.803	0.444 ± 0.012
60.605	0.590 ± 0.014	61.049	1.527 ± 0.020
62.370	0.139 ± 0.009	63.032	0.226 ± 0.010
63.489	0.067 ± 0.009	64.664	0.314 ± 0.012
66.067	0.728 ± 0.015	67.194	0.602 ± 0.015
67.836	0.644 ± 0.015	68.524	0.870 ± 0.018
69.502	1.93 ± 0.03	70.102	1.402 ± 0.023
71.530	0.094 ± 0.011	72.035	1.392 ± 0.023
72.711	1.647 ± 0.024	73.713	0.235 ± 0.013
74.131	0.266 ± 0.014	74.785	0.111 ± 0.012
75.253	1.67 ± 0.03	76.385	0.158 ± 0.013
76.818	0.301 ± 0.015	77.362	0.832 ± 0.020
78.040	0.212 ± 0.014	79.821	0.114 ± 0.013
80.396	0.290 ± 0.022	80.611	0.54 ± 0.03
80.899	1.75 ± 0.03	82.862	0.410 ± 0.018
83.309	1.37 ± 0.03	83.963	0.27 ± 0.07
84.011	0.79 ± 0.08	84.599	0.227 ± 0.016
85.267	0.92 ± 0.06	85.391	2.59 ± 0.07
86.436	0.983 ± 0.024	88.133	0.725 ± 0.023
88.740	0.819 ± 0.024	90.165	0.697 ± 0.023
91.002	0.607 ± 0.022	94.474	0.75 ± 0.03
95.081	0.105 ± 0.017	95.642	0.252 ± 0.020
97.283	1.10 ± 0.03	98.509	0.218 ± 0.020
99.280	0.402 ± 0.023	100.870	1.83 ± 0.04
101.701	1.53 ± 0.04	102.521	0.212 ± 0.021
103.830	0.44 ± 0.03	104.690	1.26 ± 0.03
106.032	0.182 ± 0.022	106.793	0.96 ± 0.05
107.022	1.12 ± 0.05	108.425	0.43 ± 0.03
109.531	0.68 ± 0.03	111.280	0.61 ± 0.03
111.831	0.60 ± 0.03	112.651	1.14 ± 0.05
112.945	4.20 ± 0.08	113.955	2.79 ± 0.06
114.731	0.24 ± 0.03	116.120	0.14 ± 0.09
116.316	4.18 ± 0.04	119.186	0.62 ± 0.04
119.507	2.04 ± 0.06	121.983	3.14 ± 0.06
123.055	14.1 ± 0.3	124.880	4.07 ± 0.08
126.037	0.34 ± 0.03	127.053	1.13 ± 0.04
129.891	0.32 ± 0.03	132.060	0.31 ± 0.03
133.064	0.18 ± 0.03	133.669	1.05 ± 0.05
134.271	0.43 ± 0.04	134.795	0.65 ± 0.04
139.162	0.84 ± 0.05	139.682	4.07 ± 0.09
140.529	0.30 ± 0.04	140.871	0.53 ± 0.05
142.862	0.28 ± 0.04	143.893	2.80 ± 0.08
144.317	2.75 ± 0.10	144.701	0.95 ± 0.06
145.705	4.35 ± 0.11	146.182	2.78 ± 0.08
147.839	1.16 ± 0.07	148.190	1.44 ± 0.07
149.436	0.43 ± 0.04	150.717	0.44 ± 0.04

TABLE V. (*Continued.*)

E_0 (eV)	$g\Gamma_n \pm \sigma_{\text{stat}}$ (meV)	E_0 (eV)	$g\Gamma_n \pm \sigma_{\text{stat}}$ (meV)
152.491	0.71 ± 0.05	153.616	2.19 ± 0.08
154.267	1.86 ± 0.07	155.065	0.52 ± 0.05
158.180	1.85 ± 0.07	158.815	0.50 ± 0.05
160.229	6.05 ± 0.15	160.612	0.96 ± 0.07
163.471	0.29 ± 0.04	164.396	2.66 ± 0.08
165.683	0.64 ± 0.06	166.120	1.01 ± 0.07
166.469	0.35 ± 0.06	167.567	3.80 ± 0.11
169.394	0.73 ± 0.05	172.200	3.60 ± 0.10
173.081	4.40 ± 0.13	174.257	2.12 ± 0.08
175.280	1.91 ± 0.08	176.326	1.89 ± 0.10
176.727	3.13 ± 0.11	179.537	1.39 ± 0.09
179.911	0.98 ± 0.08	180.470	0.63 ± 0.06
181.226	1.19 ± 0.07	182.516	0.75 ± 0.06
183.579	1.82 ± 0.09	184.070	2.21 ± 0.09
185.608	0.65 ± 0.06	186.227	1.49 ± 0.09
186.654	1.22 ± 0.08	187.517	4.42 ± 0.14
188.382	0.62 ± 0.06	189.884	0.69 ± 0.08
190.250	0.67 ± 0.08	191.064	2.04 ± 0.10
191.783	2.45 ± 0.10	192.902	5.38 ± 0.17
195.077	0.24 ± 0.05	195.821	0.72 ± 0.07
196.473	1.11 ± 0.08	197.187	3.01 ± 0.12
199.272	2.53 ± 0.11	201.999	0.52 ± 0.07
202.586	0.20 ± 0.05	204.043	0.82 ± 0.08
204.673	1.17 ± 0.08	206.078	0.92 ± 0.08
207.572	1.63 ± 0.09	208.859	2.14 ± 0.11
210.283	1.67 ± 0.13	210.640	2.05 ± 0.17
211.071	3.47 ± 0.17	212.793	0.36 ± 0.07
213.932	3.47 ± 0.14	216.325	1.25 ± 0.09
219.483	1.39 ± 0.10	220.063	0.78 ± 0.10
220.603	0.99 ± 0.10	222.118	0.41 ± 0.08
221.197	0.68 ± 0.08	222.656	0.42 ± 0.08
224.599	4.32 ± 0.17	225.471	1.82 ± 0.11
226.315	0.50 ± 0.09	226.798	1.49 ± 0.11
228.388	0.44 ± 0.07	232.332	4.45 ± 0.17
233.502	5.88 ± 0.23	235.447	0.65 ± 0.09
236.908	1.87 ± 0.12	238.468	1.08 ± 0.10
239.061	0.75 ± 0.12	239.468	1.06 ± 0.12
241.136	0.59 ± 0.09	242.239	2.10 ± 0.13
243.670	0.84 ± 0.25	243.781	1.3 ± 0.3
244.558	1.20 ± 0.11	246.467	3.24 ± 0.16
247.913	5.54 ± 0.21	248.655	2.32 ± 0.15
251.053	2.88 ± 0.16	252.214	6.0 ± 0.3
254.482	0.90 ± 0.11	255.742	12.9 ± 0.6
256.329	1.12 ± 0.13	257.622	1.53 ± 0.13
258.561	1.49 ± 0.13	259.384	7.9 ± 0.3
260.652	2.70 ± 0.16	262.868	0.58 ± 0.10
265.358	1.23 ± 0.14	265.951	3.28 ± 0.22
266.598	5.3 ± 0.3	267.837	1.64 ± 0.14
271.683	5.9 ± 0.3	272.757	1.02 ± 0.12
273.987	7.4 ± 0.3	275.076	2.55 ± 0.17
276.909	1.35 ± 0.14	277.563	1.57 ± 0.15
278.924	2.91 ± 0.19	280.013	2.55 ± 0.18
280.910	0.51 ± 0.11	281.542	1.10 ± 0.15
282.317	3.8 ± 0.3	282.897	7.8 ± 0.4
285.633	1.18 ± 0.13	288.117	4.23 ± 0.24
289.485	4.9 ± 0.3	291.076	6.2 ± 0.3
295.672	3.39 ± 0.22	298.124	1.76 ± 0.16

TABLE V. (Continued.)

E_0 (eV)	$g\Gamma_n \pm \sigma_{\text{stat}}$ (meV)	E_0 (eV)	$g\Gamma_n \pm \sigma_{\text{stat}}$ (meV)
299.693	0.97 ± 0.14	300.418	0.88 ± 0.14
301.363	1.43 ± 0.16	302.211	3.65 ± 0.24
303.571	0.66 ± 0.14	304.369	8.1 ± 0.4
307.084	1.86 ± 0.18	307.989	3.52 ± 0.24
310.268	0.69 ± 0.14	311.234	8.3 ± 0.4
312.223	1.40 ± 0.17	313.586	11.0 ± 0.6
315.387	4.7 ± 0.3	316.432	0.93 ± 0.15
317.607	2.25 ± 0.20	319.832	0.68 ± 0.14
320.986	9.6 ± 0.5	321.949	0.81 ± 0.15
325.731	0.74 ± 0.20	325.890	0.47 ± 0.22
326.558	4.0 ± 0.3	327.256	2.7 ± 0.3
328.915	0.40 ± 0.13	329.789	0.90 ± 0.18
330.480	0.96 ± 0.19	331.261	1.84 ± 0.22
332.280	4.7 ± 0.3	333.703	3.2 ± 0.3
334.963	2.8 ± 0.3	336.479	4.4 ± 0.3
337.849	1.92 ± 0.23	338.761	4.0 ± 0.3
341.211	2.55 ± 0.25	342.592	1.62 ± 0.21
344.105	1.16 ± 0.19	346.021	0.45 ± 0.14
347.545	7.5 ± 0.5	349.886	0.62 ± 0.16
350.889	2.4 ± 0.3	351.673	1.35 ± 0.20
353.935	0.47 ± 0.14	355.336	1.08 ± 0.18
357.665	2.44 ± 0.24	360.478	2.26 ± 0.24
361.742	4.4 ± 0.4	362.279	3.8 ± 0.4
363.254	1.47 ± 0.21	364.130	1.35 ± 0.22
364.859	1.50 ± 0.22	367.281	2.8 ± 0.3
368.092	1.74 ± 0.24	369.593	22.2 ± 1.6
370.875	3.6 ± 0.3	372.679	2.5 ± 0.3
373.365	1.09 ± 0.21	375.489	1.42 ± 0.21
376.691	2.4 ± 0.3	378.523	1.05 ± 0.22
379.189	3.9 ± 0.4	380.270	4.9 ± 0.4
381.400	3.1 ± 0.3	382.246	2.4 ± 0.3
384.143	2.9 ± 0.3	384.967	1.84 ± 0.25
388.234	3.3 ± 0.3	389.368	3.1 ± 0.3
390.358	0.71 ± 0.18	391.073	0.98 ± 0.20
392.314	1.66 ± 0.24	393.751	8.1 ± 0.6
395.109	0.53 ± 0.16	396.471	3.3 ± 0.4
396.987	1.5 ± 0.3	399.229	3.4 ± 0.3

background component constant in time and the sample inhomogeneities are negligible, so only the statistical uncertainty and the uncertainty due to the normalization have to be considered.

More information concerning the correlations between the different resonance parameters and the different contributions to the systematic uncertainties will be made available in EXFOR.

The ratio between the n_TOF capture cross section and the most recent evaluations is presented in Fig. 8. The ratio has been determined for the evaluations of Mughabghab (adopted for ENDF/B-VII.1), Weston (adopted in the older ENDF/B releases and similar to the previous one), and by Maslov *et al.* (adopted by the rest of the evaluations in this energy range: JEFF-3.2, JEFF-3.1 [60], JENDL-4.0, JENDL-3.3 [61], BROND-2.2 [62], and CENDL-3.1). In the 3–250 eV energy range, the n_TOF capture cross section is, on average, 6%

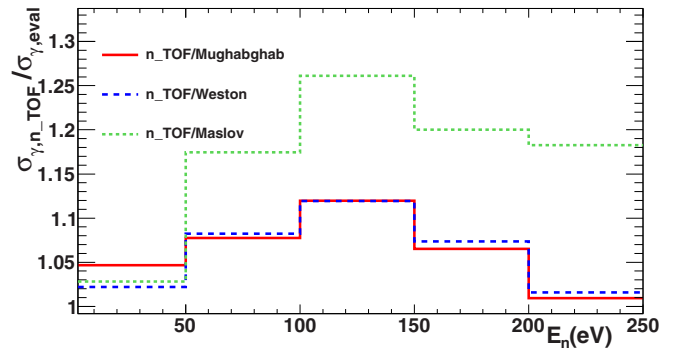


FIG. 8. (Color online) Ratio between the n_TOF capture cross section and three evaluations integrated over different energy intervals, $\int_{E_1}^{E_2} \sigma_{\gamma,n,\text{TOF}}(E)dE / \int_{E_1}^{E_2} \sigma_{\gamma,\text{eval}}(E)dE$. The low energy limit of the first bin is 3 eV, in order to avoid the strongest resonance at 1.35 eV.

larger than the Mughabghab and Weston evaluations and 13% larger than the Maslov evaluation. It should also be noted that new resonances have been found in this energy range, as well as 105 new resonances between 250 and 400 eV. In particular, the present evaluations contain 218 (Mughabghab and Weston) and 238 (Maslov) resonances up to 250 eV, whereas there are 248 resonances in the n_TOF results.

B. Statistical analysis of the resonance parameters

The average radiation width $\langle \Gamma_\gamma \rangle$ was determined from the fitted values listed in Table IV. We used the generalized weighted mean to take the correlations between different parameters into account, but very similar results are obtained if the correlations are neglected. The resonances below 3 eV were not used to calculate $\langle \Gamma_\gamma \rangle$, due to problems with sample inhomogeneities in the vicinity of the strongest resonance at 1.35 eV. The resulting value was $\langle \Gamma_\gamma \rangle = 42.00 \pm 0.12 \pm 0.5 \pm 0.3 \pm 0.7 \pm 0.6$ meV, where the uncertainties are statistical, due to the sample temperature, the background component constant in time, Doppler broadening, and sample inhomogeneities, respectively. If all the systematic uncertainties are added linearly or quadratically we obtain a total systematic uncertainty of 2.1 or 1.1 meV, respectively.

An estimation of the *s*-wave average level spacing D_0 can be obtained, in principle, from $D_0 = \Delta E / (N - 1)$ and $\Delta D_0 / D_0 \approx 1/N$ [63], where N is the number of resonances observed in the neutron energy interval between E_1 and E_2 and $\Delta E = E_2 - E_1$. However, there are usually a certain number of small resonances which have not been detected (missing resonances), and their number has to be estimated as well. One of the most common methods is based on assuming that the values of the reduced neutron widths $\Gamma_n^0 = \Gamma_n \times (E_0/1 \text{ eV})^{-1/2}$ are distributed, for each spin value J , according to a Porter-Thomas distribution with one degree of freedom $p(x)dx = e^{-x^2/2} / \sqrt{2\pi x}$, where $x = \Gamma_{n,J}^0 / \langle \Gamma_{n,J}^0 \rangle$. Since the spins of the resonances have not been determined, we assumed that $1/D_{0,J} \propto (2J + 1)$ and that $S_{0,J} = S_0$ (both assumptions are justified in Appendix D of [64]), where $S_0 = \langle g\Gamma_n^0 \rangle / D_0$ is the *s*-wave neutron strength function. From

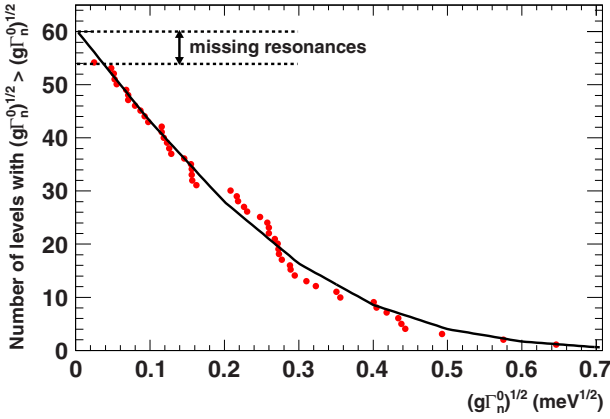


FIG. 9. (Color online) Estimation of the number of missing resonances, performed in the 0–40 eV energy range. The experimental points were fitted to Eq. (2).

these assumptions it follows that $\langle g_J \Gamma_{n,J}^0 \rangle = \langle g \Gamma_n^0 \rangle$, i.e., the value of $\langle g \Gamma_n^0 \rangle$ is the same for both spin groups. Therefore, it is possible to consider only one Porter-Thomas distribution, where both spin groups are included, after making the change of variable from $x = \Gamma_n^0 / \langle \Gamma_n^0 \rangle$ to $y = g \Gamma_n^0 / \langle g \Gamma_n^0 \rangle$. With some manipulations of the Porter-Thomas distribution, it follows that, for a given energy interval, the number of resonances with $\sqrt{g \Gamma_n^0}$ greater than a certain value, x , is obtained from

$$f(x) = N \frac{2}{\sqrt{\pi} \sqrt{2 \langle g \Gamma_n^0 \rangle}} \int_x^\infty \exp\left(-\frac{y^2}{2 \langle g \Gamma_n^0 \rangle}\right) dy, \quad (2)$$

where N is the number of resonances in the energy interval. This formula was used to estimate the number of missing resonances, by fitting the values of N and $\langle g \Gamma_n^0 \rangle$, as it is presented in Fig. 9. The result was $D_0 = 0.66(3)$ eV, where the uncertainty was estimated from the statistical uncertainty due to the number of resonances considered and from the differences observed in the calculation of D_0 in different neutron energy intervals.

The neutron strength function for s -wave resonances S_0 can be obtained from $S_0 = \sum_\lambda g \Gamma_{n,\lambda}^0 / \Delta E$ and $\Delta S_0 / S_0 = \sqrt{2/N}$ [63], and was calculated from the slope of the experimental cumulative sum, as it is presented in Fig. 10. The result was $S_0 = 1.08(8) \times 10^{-4}$, with an additional 3% normalization uncertainty.

C. Analysis of the unresolved resonance region

We have treated the energy range between 250 and 2500 eV as the unresolved resonance region (URR). Thus, the 250–400 eV energy region has been analyzed as both RRR and URR, the latter for comparison to the existing experiments and evaluations. The analysis has been performed with SAMMY, which contains a modified version of the FITACS code [39,65], which uses Hauser-Feshbach theory [66] with width fluctuations.

SAMMY performs the fits in the URR to the capture cross section instead of the capture yield. In the URR the self-shielding and multiple scattering effects are negligible, so

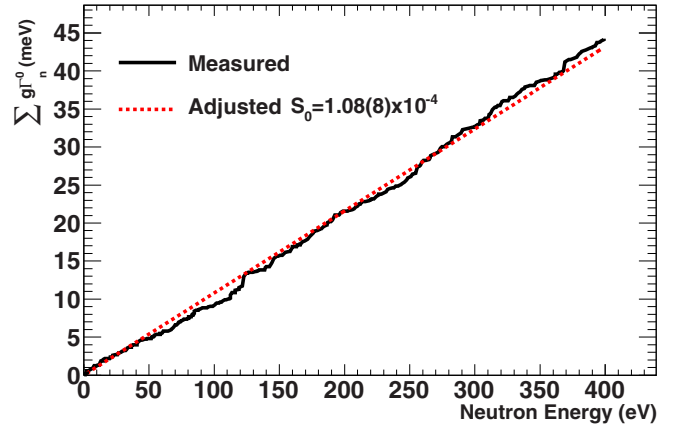


FIG. 10. (Color online) Linear fit of $\sum_\lambda g \Gamma_{n,\lambda}^0$ as a function of the neutron energy.

σ_γ was obtained directly by dividing the capture yield by the sample thickness, $\langle \sigma_\gamma(E_n) \rangle = \langle Y_\gamma(E_n) \rangle / n$. In the calculation of the capture yield, the background was subtracted without any smoothing procedure, since it cannot be verified if the smoothed background is at the level of the measured yield between resonances, as it can be done in the RRR. Concerning the uncertainties, all the contributions to the systematic uncertainties mentioned in Sec. IV A are negligible in this energy range, with the exception of the uncertainty in the normalization. The largest contribution to the statistical uncertainties comes from the subtraction of the measured background.

The only parameters which could be fitted with the n_TOF data were S_0 and the s -wave radiation width $\langle \Gamma_\gamma \rangle_0$. The channel radius, distant level parameter R_l^∞ and fission parameters are not sensitive to this measurement, and the p -wave contribution starts to be important at higher energies. In particular, according to the ENDF/B-VII.1 evaluation, the p -wave contribution to the total capture cross section is around 11% at 2.5 keV, and a variation of 25% in the S_1 value induces a change of only 0.5% in the fitted value of S_0 .

The fit of S_0 and $\langle \Gamma_\gamma \rangle_0$ was performed by using the results of the statistical analysis of the RRR as prior uncertainties, and the average level spacing was fixed to the obtained value ($D_0 = 0.66$ eV). The results of the fit were $S_0 = 1.10(4) \times 10^{-4}$ and $\langle \Gamma_\gamma \rangle_0 = 42.1(20)$ meV, with a correlation between them of -0.23 . All these uncertainties and correlations are statistical, and there is an extra systematic uncertainty of 3% in the S_0 value due to the uncertainty in the normalization. If no prior knowledge of the parameters is assumed, compatible values of S_0 and $\langle \Gamma_\gamma \rangle_0$ are obtained, but with larger uncertainties and correlations.

The fit to the n_TOF capture data are compared in Fig. 11 with the only two available capture data sets in this energy range, tagged as “Weston I” [67] and “Weston II” [68]. Both of them have been provided by Weston *et al.* (see Table I), in the range from 250 eV up to 92 keV and differ significantly below 1.5–2 keV. The n_TOF data are compatible, in absolute value and shape, with the Weston I data set, whereas they are not with the Weston II data. This is an

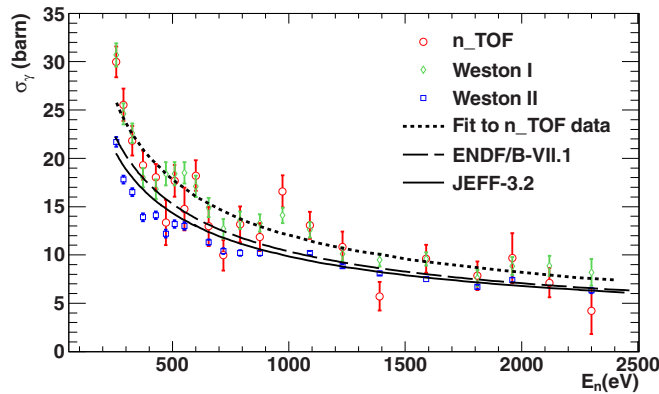


FIG. 11. (Color online) Fitted n_TOF capture data in the URR together with the two different data sets provided by Weston *et al.*, in their common energy range, and with the cross sections provided by the ENDF/B-VII.1 and JEFF-3.2 evaluations.

important result, since the normalization of the n_TOF data to the available transmission experiments has been performed at lower energies. On the other hand, all present evaluations, which do not differ significantly from the two cases in Fig. 11, are much closer to the Weston II data set, underestimating the ^{243}Am capture cross section in this energy region between 7% and 20%.

D. Analysis at higher energies

The high energy limit of the n_TOF data is 2.5 keV. However, we have used the experimental data available in EXFOR and in the literature to extend the analysis up to higher energies.

The URR ranges up to 40–42 keV in the present evaluations. As it is shown in Table I, there are two measurements available in EXFOR which can be used to extend the analysis of the URR to higher energies: the one by Weston *et al.* (above 2 keV the two datasets provided by Weston *et al.* are compatible) and the one by Wisshak *et al.*, which is 10–15% below the Weston *et al.* measurement, but exhibits a similar shape. We think that there are two reasons to prefer the normalization of Weston *et al.* First, it is compatible with the n_TOF results in their common energy range. Second, the Wisshak *et al.* data are not compatible with the PROFIL-1 integral measurement, which is presented below. For this reason, we performed a fit to the Weston *et al.* data in the 2.5–42 keV energy range by varying S_1 and $\langle\Gamma_\gamma\rangle_1$, with the values of S_0 and $\langle\Gamma_\gamma\rangle_0$ fixed to the results obtained from the n_TOF data analysis. The results were $S_1 = 1.65(24) \times 10^{-4}$ and $\langle\Gamma_\gamma\rangle_1 = 52(34)$ meV, with a correlation of -0.82 . No systematic uncertainties were included in the calculations, since their description in Ref. [8] is not detailed enough, and thus only the statistical uncertainties available in EXFOR were taken into account.

The obtained URR parameters are presented together with those obtained in other experiments and evaluations in Table VI. Note that in all cases the parameter values are at zero neutron energy, $E_n = 0$, and in the case of the n_TOF data the evolution of the URR parameters with E_n is the one described in Ref. [39]. The ratio between the results obtained

TABLE VI. URR parameters (at $E_n = 0$) obtained in this work compared with the ones obtained in other evaluations.

	D_0 (eV)	S_0 (10^{-4})	$\langle\Gamma_\gamma\rangle_0$ (meV)	S_1 (10^{-4})	$\langle\Gamma_\gamma\rangle_1$ (meV)
This work	0.66(3)	1.10(5) ^a	42.1(20)	1.65(24) ^b	52(34) ^b
Belanova	0.62	0.65			
Berreth			42		
Simpson	0.68	0.96(10)	39		
Cote			43(3)		
RIPL-3 [63]	0.73(6)	0.98(6)	39(3)		
Mughabghab	0.60(6)	0.98(9)	39(1)		
Maslov ^c	0.57(5)	0.87(15)	43	2.176	43
BROND-2.2	0.67	0.93	39	2.44	39
JENDL-4.0	0.44	0.864	39	2.687	39
ENDF/B-VII.0	0.75	0.98	39	2.2	44
ENDF/B-VII.1	0.66	0.98	39.1	2.6	69.8

^aThis uncertainty has been obtained by adding quadratically the statistical uncertainty (0.04×10^{-4}) to the 3% systematic uncertainty due to the normalization.

^bValues obtained from the n_TOF +Weston *et al.* measurements.

^cValues adopted by the JEFF-3.2, JEFF-3.1, JENDL-3.3, and CENDL-3.1 evaluations.

in this work (from the data of n_TOF and Weston *et al.*) and the capture cross sections of different evaluations are presented in Fig. 12. Note that the cross section obtained in this work is similar in shape to the one of the ENDF/B-VII.0 library, but 10–12% larger.

In addition to the differential measurements of Weston *et al.* and Wisshak *et al.*, there are integral capture measurements in the fast energy range that can be considered for constraining the capture cross section. In the PROFIL-1 experiment, an ^{243}Am sample was irradiated in the fast PHENIX reactor in 1974 [19,20]. In fact, the changes in the ENDF/B-VII.1 evaluation with respect to ENDF/B-VII.0 were motivated by the results of this integral experiment [14]. The information which can be obtained from PROFIL-1 is the effective capture cross section of ^{243}Am , $\sigma_{\text{cap}} = \int \phi(E)\sigma_\gamma(E)dE$, where $\phi(E)$ is the neutron

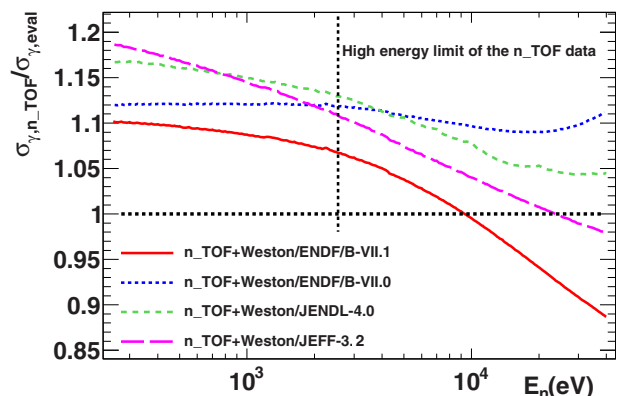


FIG. 12. (Color online) Ratio between the n_TOF fitted capture cross section and the ones available in different evaluations. JEFF-3.2 is the same as JEFF-3.1, JENDL-3.3, and CENDL-3.1, in this energy range.

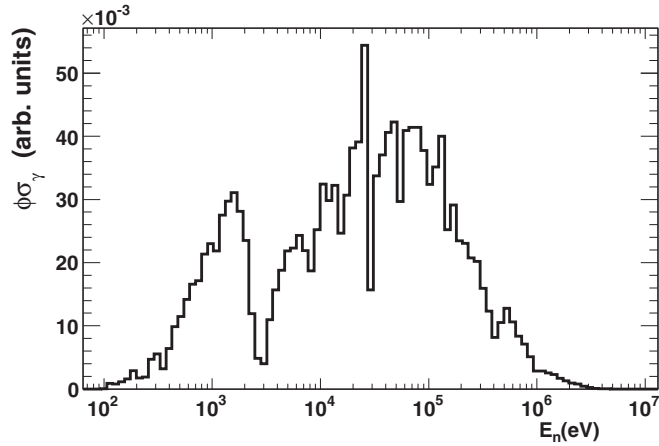


FIG. 13. PROFIL-1 neutron flux multiplied by the ^{243}Am capture cross section in the JEFF-3.2 library.

flux at the irradiated sample position. As we had access to the shape of the mentioned neutron flux, obtained from detailed Monte Carlo simulations [69], we used this flux to compare the experimental values of PROFIL-1 with the ones calculated from different capture cross sections. The neutron flux used in these calculations multiplied by the ^{243}Am capture cross section is presented in Fig. 13, in order to show the neutron energy ranges sensitive to the PROFIL-1 integral experiment.

References [19,20] provide calculated to experimental ratios (C/E) of the effective capture cross section, σ_{cap} , each calculated with a different neutron data library. We did not have enough information to calculate these C/E values, but with the shape of the neutron flux we could calculate ratios between σ_{cap} values obtained from different libraries, i.e., we could calculate ratios between different C/E values. We used the C/E value provided by [20] with the ENDF/B-VII.0 evaluated library to normalize our results. With this normalization, we calculated the C/E values using several evaluated data libraries, and the results obtained are presented in the second column of Table VII. It was found that the results are in reasonable agreement with the values provided by [20] and [19], shown in the third and fourth columns. This indicates that the neutron flux used in this work is similar to the ones used by the references.

In a second step, we constructed several ^{243}Am capture cross sections by taking the results obtained from the analysis of the n_TOF+Weston data up to 42 keV (end of the URR in most of the evaluated libraries), and the energy regions above 42 keV present in the different evaluated libraries. The corresponding C/E values obtained with these cross sections (with the previously mentioned normalization) are presented in the right column of Table VII. The experimental result has an estimated uncertainty of 5%, so we considered that only the results obtained with the high energy regions of the ENDF/B-VII.1, JEFF-3.2, JEFF-3.0 [70], and CENDL-3.1 libraries are in reasonable agreement with the PROFIL-1 integral experiment. Note that all the C/E values presented in Table VII are smaller than unity.

On the other hand, if the data of Wisshak *et al.* are normalized to the Weston *et al.* data in their common energy

TABLE VII. C/E values of the PROFIL-1 irradiation experiment obtained with different libraries (second column), the same values provided by the references (third and fourth columns), and the C/E values obtained from the capture cross section resulting from taking the RRR and URR of this work and the part above 42 keV from the corresponding evaluated library.

	Library	[20]	[19]	This work
ENDF/B-VII.1	0.934	0.939		0.939
ENDF/B-VII.0	0.834 ^a	0.834	0.85	0.889
JENDL-4.0	0.852			0.904
JEFF-3.2 ^b	0.892			0.929
JEFF-3.0	0.936		0.99	0.959
CENDL-3.1	0.911			0.947
ROSFOND-2010	0.801			0.860
ENDF/B-V.0	0.585		0.62	0.730

^aValue fixed to the value provided in Ref. [20] for normalization purposes. The rest of the values of this column were obtained from this value and the calculated C/E ratios.

^bSame as JEFF-3.1 and JENDL-3.3.

range (which is reasonable, since n_TOF is compatible with Weston *et al.* and because the Wisshak *et al.* data are not compatible with the results of the PROFIL-1 irradiation experiment), the capture cross sections provided by ENDF/B-VII.1 (below 100 keV) and by JEFF-3.0 (above 100 keV) are not compatible with the differential data, whereas the high energy regions ($E_n > 42$ keV) of the JEFF-3.2 and the CENDL-3.1 libraries are.

In conclusion, the ^{243}Am capture cross section constructed from the RRR and URR obtained in this work up to 42 keV and the JEFF-3.2 or the CENDL-3.1 evaluations above 42 keV is in agreement with both the PROFIL-1 and the currently available differential capture data. In particular, this constructed cross section (1) fits the n_TOF data between 0.7 eV and 2.5 keV; (2) fits the mentioned “Weston I” data between 0.25 and 2.5 keV; (3) fits both Weston *et al.* data sets between 2.5 and 42 keV; (4) fits the Wisshak *et al.* data up to 250 keV, if they are normalized to the Weston *et al.* data; (5) is compatible with the integral experimental results of the PROFIL-1 irradiation experiment; and (6) there is a continuous match between the URR and the high energy region, at 42 keV.

V. CONCLUSIONS

The ^{243}Am capture cross section has been measured at n_TOF using the segmented BaF₂ total absorption calorimeter (TAC), in the energy range between 0.7 and 2500 eV.

The certified mass of the ^{243}Am sample provided by the manufacturers was not correct, and therefore we normalized the n_TOF capture cross section to the existing transmission measurements in the neutron energy range between 3 and 50 eV. This normalization was consistent with the sample mass obtained from a high resolution γ -ray spectrometry analysis and a low resolution measurement performed with the TAC of the sample activity. In addition, this normalization is consistent with one of the only two capture measurements in the 250–2500 eV energy interval available in EXFOR.

Due to the large flight path of the n_TOF facility (185 m) and the statistics achieved, the results provide, with the exception of 1.35 eV resonance, a better description of the resolved resonance parameters (energy, $g\Gamma_n$, Γ_γ) than the ones available in current data libraries, which were obtained essentially from a single transmission measurement. The uncertainties in the resonance parameters have been reduced, new resonances have been found and the resolved resonance region has been extended from 250 eV up to 400 eV.

The value of the resonance integral, $I_0 = \int_{0.5\text{ eV}}^{\infty} \sigma_\gamma(E)/E dE$, obtained in this work is significantly lower than the rest of the measured values. The strongest resonance at 1.35 eV contributes in 70–80% to the value of I_0 , and the existence of inhomogeneities in the sample, which would affect the self-shielding and multiple scattering corrections in this resonance, can explain this difference. The self-shielding corrections in the rest of the resonances are very small and have no significant effect on the resulting resonance parameters.

In the unresolved resonance region, it has been found that the n_TOF results are compatible with one of the two available capture measurements in the 0.25–2.5 keV energy range. Due to the fact that the current evaluations are closer to the other capture measurement, they underestimate the $^{243}\text{Am}(n,\gamma)$ cross section by 7–20% in the mentioned energy range.

We have completed the $^{243}\text{Am}(n,\gamma)$ cross section analysis above 2.5 keV by using the data available in EXFOR and in the literature, including both differential and integral measurements. In particular, we have found an $^{243}\text{Am}(n,\gamma)$ cross section that reproduces, under some assumptions, all the differential data sets and the PROFIL-1 integral experiment.

Taking into account the n_TOF measurement, the main uncertainties of the $^{243}\text{Am}(n,\gamma)$ cross section refer to thermal energies, to the strongest resonance at 1.35 eV, and to the fast energy range for reactor applications. The experimental results of Jandel *et al.* [10] and Hori *et al.* [11], which have not been published yet, could reduce some of these uncertainties.

ACKNOWLEDGMENTS

This work has been supported by ENRESA under the CIEMAT-ENRESA agreement on the “Separación y Transmutación de Residuos Radiactivos”, the Spanish National Plan I+D+I of the Spanish Ministry of Economy and Competitiveness (project no. FPA2011-28770-C03-01), the European Commission 6th Framework Programme project IP-EUROTRANS (F16W-CT-2004-516520), and the CONSOLIDER-INGENIO project no. CSD-2007-00042.

-
- [1] *One possible optimization for target accuracy for innovative systems using recent covariance data evaluations*, Technical Report No. 6410, edited by M. Salvatores and R. Jacqmin (NEA/WPEC-26, Vienna, Austria, 2008).
- [2] G. Aliberti, G. Palmiotti, M. Salvatores, and C. G. Stenberg, *Nucl. Sci. Eng.* **146**, 13 (2004).
- [3] G. Aliberti, G. Palmiotti, M. Salvatores, T. K. Kim, T. A. Taiwo, M. Anitescu, I. Kodeli, E. Sartori, J. C. Bosq, and J. Tommasi, *Ann. Nucl. Energy* **33**, 700 (2006).
- [4] T. S. Belanova, A. G. Kolesov, V. A. Poruchikov, G. A. Timofeev, S. M. Kalebin, V. S. Artamonov, and R. N. Ivanov, *At. Energ.* **40**, 298 (1976).
- [5] O. D. Simpson, F. B. Simpson, J. A. Harvey, G. G. Slaughter, R. W. Benjamin, and C. E. Ahlfeld, *Nucl. Sci. Eng.* **55**, 273 (1974).
- [6] J. R. Berreth and F. B. Simpson, Idaho Nuclear Corp. Reports **1407**, 66 (1970).
- [7] R. E. Coté, L. M. Bollinger, R. F. Barnes, and H. Diamond, *Phys. Rev.* **114**, 505 (1959).
- [8] L. W. Weston and J. H. Todd, *Nucl. Sci. Eng.* **91**, 444 (1985).
- [9] K. Wisshak and F. Käppeler, *Nucl. Sci. Eng.* **85**, 251 (1983).
- [10] M. Jandel, T. A. Bredeweg, M. A. Stoyer, C. Y. Wu, M. M. Fowler, J. A. Becker, E. M. Bond, A. Couture, R. C. Haight, R. J. Haslett, R. A. Henderson, A. L. Keksis, J. M. O'Donnell, R. S. Rundberg, J. L. Ullmann, D. J. Vieira, J. B. Wilhelmy, and J. M. Wouters, *AIP Conf. Proc.* **1090**, 220 (2009).
- [11] J. Hori, M. Oshima, H. Harada, K. Furutaka, M. Koizumi, F. Kitatani, Y. Toh, S. Nakamura, A. Kimura, M. Igashira, M. Mizumoto, T. Ohsaki, T. Katabuchi, and J. Goto, in *Proceedings of the 2008 Annual Symposium on Nuclear Data (NDS 2008)*, JAEA-CONF 2009-004, edited by S. CHIBA (Ricotti, Tokai, Japan, 2009), p. 123.
- [12] A. Kimura *et al.*, *J. Nucl. Sci. Technol.* **49**, 708 (2012).
- [13] A. Alekseev, A. Bergman, A. Berlev, E. Koptelov, A. Egorov, B. Samylin, B. Fursov, and V. Shorin, *At. Energ.* **111**, 428 (2012).
- [14] M. Chadwick *et al.*, *Nucl. Data Sheets* **112**, 2887 (2011), special issue on ENDF/B-VII.1 Library.
- [15] K. Shibata, O. Iwamoto, T. Nakagawa, N. Iwamoto, A. Ichihara, S. Kunieda, S. Chiba, K. Furutaka, N. Otuka, T. Ohsawa, T. Murata, H. Matsunobu, A. Zukeran, S. Kamada, and J. Katakura, *J. Nucl. Sci. Technol.* **48**, 1 (2011).
- [16] The JEFF team, JEFF-3.2: Evaluated nuclear data library, Technical Report 2014.
- [17] Rosfond-2010 library, 2010.
- [18] Z. G. Ge, Y. X. Zhuang, T. J. Liu, J. S. Zhang, H. C. Wu, Z. X. Zhao, and H. Xia, *J. Korean Phys. Soc.* **59**, 1052 (2011).
- [19] G. Palmiotti, G. Aliberti, M. Salvatores, and J. Tommasi, *AIP Conf. Proc.* **769**, 1436 (2005).
- [20] A. Kahler, R. MacFarlane, R. Mosteller, B. Kiedrowski, S. Frankle, M. Chadwick, R. McKnight, R. Lell, G. Palmiotti, H. Hiruta, M. Herman, R. Arcilla, S. Mughabghab, J. Sublet, A. Trkov, T. Trumbull, and M. Dunn, *Nucl. Data Sheets* **112**, 2997 (2011), special issue on ENDF/B-VII.1 Library.
- [21] M. Chadwick *et al.*, *Nucl. Data Sheets* **107**, 2931 (2006), evaluated Nuclear Data File ENDF/B-VII.0.
- [22] F. Marie, A. Letourneau, G. Fioni, O. Druelle, C. Veysseyre, H. Faust, P. Mutti, I. Al Mahamid, and B. Muhammad, *Nucl. Instrum. Methods Phys. Res. A* **556**, 547 (2006).
- [23] M. Ohta, S. Nakamura, H. Harada, T. Fujii, and H. Yamana, *J. Nucl. Sci. Technol. (Tokyo)* **43**, 1441 (2006).
- [24] Y. Hatsukawa, N. Shinohara, and K. Hata, in *JAERI Conference Proceedings of the 1997 Symposium on Nuclear Data*, edited by T. Yoshida and T. Fukahori (Japan Atomic Energy Agency, Japan, 1998), Vol. 98.003, p. 221.

- [25] V. D. Gavrilov, V. A. Goncharov, V. V. Ivanenko, V. N. Kustov, and V. P. Smirnov, *At. Energ.* **41**, 185 (1976).
- [26] S. H. Eberle, W. Robel, W. Jung, I. Bayat, H. J. Bleyl, E. Bojarsky, L. Schmidt, E. Gantner, J. Reinhardt, and C. Krueckeberg, *Actinides Project. First Half-Year Report*, Technical Report No. 1456 (Karlsruhe Institute of Technology, Germany, 1971), p. 45.
- [27] R. L. Folger, J. A. Smith, L. C. Brown, R. F. Overman, and H. P. Holcomb, in *Proceedings of a Conference on Neutron Cross Sections and Technology*, edited by D. T. Goldman (U.S. National Bureau of Standards, Washington D. C., 1968), Vol. 2, p. 1279.
- [28] M. A. Bak, A. S. Krivokhatskii, K. A. Petrzhak, Y. G. Petrov, Y. F. Romanov, and E. A. Shlyamin, *At. Energ.* **23**, 316 (1967).
- [29] C. H. Ice, Production of the transplutonium elements at Savannah River., Technical Report No. 66, Du Pont, Savannah River Reports.
- [30] J. P. Butler, M. Lounsbury, and J. S. Merritt, *Can. J. Phys.* **35**, 147 (1957).
- [31] B. G. Harvey, H. P. Robinson, S. G. Thompson, A. Ghiorso, and G. R. Choppin, *Phys. Rev.* **95**, 581 (1954).
- [32] C. M. Stevens, M. H. Studier, P. R. Fields, J. F. Mech, P. A. Sellers, A. M. Friedman, H. Diamond, and J. R. Huizenga, *Phys. Rev.* **94**, 974 (1954).
- [33] S. F. Mughabghab, *Atlas of Neutron Resonance Resonance Parameters and Thermal Cross Sections Z = 1-100* (Elsevier, New York, 2006).
- [34] O. Schwerer, *EXFOR Format Description for Users*, Technical Report No. 206 (IAEA Nuclear Data Section, Vienna, Austria, 2008).
- [35] U. Abbondanno *et al.* (tn_TOF Collaboration), *CERN n_TOF Facility: Performance Report*, Technical Report No. INTC-2002-037 (CERN, 2003).
- [36] F. Gunsing *et al.*, *Nucl. Instrum. Methods Phys. Res. B* **261**, 925 (2007).
- [37] The n_TOF facility was closed at the end of the 2004 campaign. It was opened again in 2009 (Phase-2), with a different lead block and coolant circuit.
- [38] J. Pancin *et al.* (n_TOF Collaboration), *Nucl. Instrum. Methods Phys. Res. A* **524**, 102 (2004).
- [39] N. Larsson, Updated User's Guide for SAMMY: Multilevel R-matrix Fits to Neutron Data Using Bayes Equations, Technical Report No. ORNL/TM-9179/R7.
- [40] S. Marrone *et al.*, *Nucl. Instrum. Methods Phys. Res. A* **517**, 389 (2004).
- [41] C. Guerrero *et al.* (n_TOF Collaboration), *Nucl. Instrum. Methods Phys. Res. A* **608**, 424 (2009).
- [42] U. Abbondanno *et al.* (n_TOF Collaboration), *Nucl. Instrum. Methods Phys. Res. A* **538**, 692 (2005).
- [43] E. Berthoumieux, Preliminary Report on BaF2 Total Absorption Calorimeter Test Measurement, Technical Report (CEA-Saclay/DAPNIA/SPhN, 2004).
- [44] S. Marrone *et al.*, *Nucl. Instrum. Methods Phys. Res. A* **568**, 904 (2006).
- [45] C. Massimi *et al.* (n_TOF Collaboration), *Phys. Rev. C* **81**, 044616 (2010).
- [46] C. Guerrero *et al.* (n_TOF Collaboration), *Phys. Rev. C* **85**, 044616 (2012).
- [47] E. Mendoza *et al.* (n_TOF Collaboration), "Pulse pile-up and dead time corrections for digitized signals from a BaF₂ calorimeter", (2014), *Nucl. Instrum. Methods Phys. Res. A* (submitted).
- [48] Data buffers of different measurements, which cannot have exactly the same energy calibration, are added artificially to perform the pile-up corrections (see [47]).
- [49] J. Tain and D. Cano-Ott, *Nucl. Instrum. Methods Phys. Res. A* **571**, 719 (2007).
- [50] S. Agostinelli *et al.* (GEANT4 Collaboration), *Nucl. Instrum. Methods Phys. Res. A* **506**, 250 (2003).
- [51] C. Guerrero, D. Cano-Ott, E. Mendoza, J. Taín, A. Algora, E. Berthoumieux, N. Colonna, C. Domingo-Pardo, E. González-Romero, M. Heil, D. Jordán, F. Käppeler, C. Lampoudis, T. Martínez, C. Massimi, and R. Plag, *Nucl. Instrum. Methods Phys. Res. A* **671**, 108 (2012).
- [52] E. Mendoza *et al.* (n_TOF Collaboration), "The Am-243 neutron capture measurement at the n_toF facility", in *Capture Gamma-Ray Spectroscopy and Related Topics* (World Scientific, Singapore, 2013), Chap. 60, pp. 442–449, http://www.worldscientific.com/doi/pdf/10.1142/9789814383646_0060.
- [53] E. Mendoza, Ph.D. thesis, Universidad Complutense de Madrid, 2014.
- [54] R. L. Macklin, J. Halperin, and R. R. Winters, *Nucl. Instrum. Methods* **164**, 213 (1979).
- [55] V. M. Maslov, E. S. Sukhovitskij, Y. V. Porodzinskij, A. B. Klepatskij, and G. B. Morogovskij, Evaluation of neutron data for Americium-243, Technical Report No. INDC(BLR)-006 (IAEA, 1996).
- [56] Simpson *et al.*, file EXFOR 10204.004, retrieved from the IAEA Nuclear Data Services website.
- [57] Simpson *et al.*, file EXFOR 10204.005, retrieved from the IAEA Nuclear Data Services website.
- [58] The energy ranges considered were, in eV: 3-50, 3-25, 3-10, 8.5-12.5, 10-17 and 14-25.
- [59] S. Oh and L. C. Leal, SUGGEL: A Program Suggesting The Orbital Angular Momentum of a Neutron Resonance from the Magnitude of its Neutron Width, Technical Report No. ORNL/TM-2000/314.
- [60] OECD/NEA Data Bank, The JEFF-3.1 Nuclear Data Library, JEFF Report 21, Technical Report (2006).
- [61] K. Shibata *et al.*, *J. Nucl. Sci. Technol.* **39**, 1125 (2002).
- [62] BROND-2.2, Russian Evaluated Neutron Reaction Data Library, Technical Report No. IAEA-NDS-90 Rev.8, 1994, edited by A. I. Blokhin, A. V. Ignatyuk, V. N. Manokhin, M. N. Nikolaev, and V. G. Pronyaev.
- [63] R. Capote *et al.*, *Nucl. Data Sheets* **110**, 3107 (2009).
- [64] A. Trkov, M. Herman, and D. A. Brown, ENDF-6 Formats Manual: Data Formats and Procedures for the Evaluated Nuclear Data Files ENDF/B-VI and ENDF/B-VII, Technical Report No. BNL-90365-2009 Rev.2.
- [65] F. H. Fröhner, *Nucl. Sci. Eng.* **103**, 119 (1989).
- [66] W. Hauser and H. Feshbach, *Phys. Rev.* **87**, 366 (1952).
- [67] Weston *et al.*, file EXFOR 12951.002, retrieved from the IAEA Nuclear Data Services website.
- [68] Weston *et al.*, file EXFOR 12951.003, retrieved from the IAEA Nuclear Data Services website.
- [69] D. Villamarín (personal communication).
- [70] OECD/NEA Data Bank, The JEFF-3.0 Nuclear Data Library, JEFF Report 19, Technical Report (2005).